Project objectives for the period

Concept and project objective(s)

The balance between bone resorption and bone formation determines the mass and structural integrity of the skeleton and is disturbed in osteoporosis. Current therapies of osteoporosis, with the exception of PTH, prevent bone loss and protect its microarchitecture but cannot activate bone formation. Understanding the mechanisms regulating bone formation can lead to treatments able to rebuild bone mass and architecture. In recent years identification of the molecular defects of rare bone disorders characterized by high bone mass of good quality have led to the recognition of the critical role of LRP5, a co-receptor of Wnt signalling, in the regulation of bone formation. These observations have opened a new area of investigation in the molecular mechanisms of osteoblast-mediated bone formation and consequently in the development of therapeutics for osteoporosis by targeting the Wnt signalling pathway. In this research proposal we plan to perform studies with the following objectives:

- To characterize the clinical, biochemical, radiological and histological features of patients with craniotubular hyperostoses, especially those with sclerosteosis and van Buchem disease.
- To determine the genetic defect in patients with craniotubular hyperostosis and to establish putative genotype-phenotype correlations.
- To determine the mechanism by which sclerostin inhibits bone formation and to determine how genetic variations in SOST, LRP5 and Wnt signalling pathway modify bone architecture and remodelling and osteocyte density.
- To reveal the pattern of sclerostin expression by analysis of the SOST promoter and by histomorphometric analysis of bone biopsies taken from patients with osteoporosis, osteoarthritis and controls.
- To elucidate the interaction of sclerostin with LRP5 and to identify and characterize co-factors of LRP5 signalling and their in vivo action in relevant animal models.
- To identify epitopes in sclerostin that mediate the interactions with LRP5 (and vise versa) and to raise peptide-bound protein mimics and antibodies that interfere with sclerostin/LRP5 interactions and test them in vitro and in animal models of bone loss.

Progress beyond the state of the art

Bone is a highly specialized connective tissue that is renewed throughout life. In the adult old bone is replaced by new bone in the same location, a process known as bone remodelling. This occurs in an orderly fashion through temporary anatomic structures called basic multicellular units (BMUs).[1]
A BMU comprises a team of osteoclasts in the front and a team of osteoblasts in the back supported by blood vessels, nerves and connective tissue. Osteoclasts resorb bone while osteoblasts move to the resorbed area and lay down new bone matrix that subsequently mineralizes, a sequence known as coupling. The balance between the supply of new cells and their life span are critical for the maintenance of bone homeostasis, is controlled by hormones, cytokines and mechanical factors and is disturbed in bone diseases. In osteoporosis, the most common bone disease, the bone remodelling balance is disturbed leading to reduced bone mass and deterioration of bone architecture resulting in increased bone fragility and risk of fractures. The molecular mechanisms regulating bone resorption have been identified and agents that reduce bone resorption are currently the most widely used therapeutics in the management of osteoporosis. These agents reduce the rate of bone remodelling, preserve its microarchitecture and reduce the risk of fractures in patients with osteoporosis. However, they cannot increase bone mass and rebuild bone architecture. This can only be done by stimulating bone formation by osteoblasts. In contrast to our current understanding of the molecular mechanisms regulating bone resorption, knowledge of the mechanisms regulating bone formation has lagged behind mainly because of lack of suitable experimental approaches. A recent breakthrough has been the identification of a link between bone mass in humans with rare skeletal disorders and gain- or loss-of-function mutations of the Wnt co-receptor LRP5 or of the Wnt antagonist sclerostin.[2]

LRP5 is involved in canonical Wnt signalling where it acts as a co-receptor for Wnt ligands to

regulate intracellular signal transduction by β-catenin. Recent advances in bone biology emphasize the importance of the canonical Wnt signalling pathway during osteoblast differentiation in embryonic development and for osteoblast maturation and activity during postnatal life. Structurally LRP5 consists of a large extracellular domain, a single transmembrane-spanning segment and a cytoplasmic tail. Different proteins can bind to the extracellular portion of LRP5, thereby regulating the activity of the canonical Wnt signalling pathway (Figure 1). Dickkopfs (DKKs) comprise one family of proteins that inactivate the signalling cascade by direct binding to LRP5 and/or its homologue LRP6 receptors. Sclerostin, a protein expressed in the adult skeleton exclusively in osteocytes,[3,4] antagonizes Wnt signalling by interacting with LRP5 via an currently unknown mechanism of action that appears to differs from that of DKKs.[5,6]

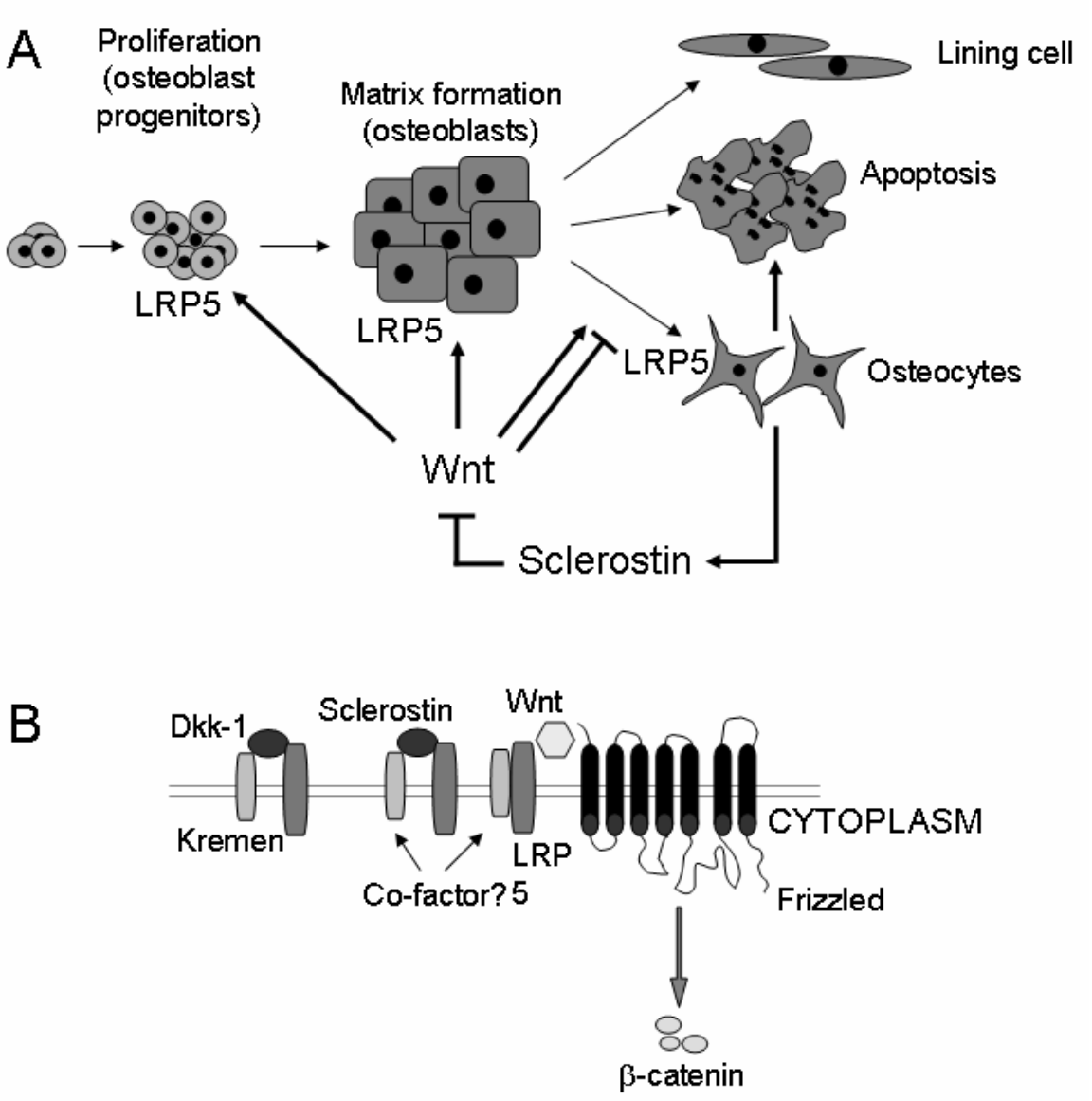

Figure 1. Wnt signalling in osteogenesis. A) Simplified scheme of the effect of Wnts on osteogenesis and its regulation by sclerostin. B) Simplified scheme of some key players of Wnt signalling, especially addressing the Wnt antagonist Dkk1 and sclerostin.

Loss-of-function mutations of LRP5 result in the osteoporosis pseudoganglioma syndrome characterized by congenital blindness and osteoporosis, while gain-of-function mutations cause high bone density phenotypes.[7-9] Sclerosteosis and van Buchem disease are rare autosomal recessive skeletal dysplasias characterized by progressive sclerosis of the skeleton.[10] These and other craniotubular hyperostoses including autosomal dominant forms differentially diagnosed as “high bone

mass" (HBM) phenotype, osteosclerosis, endosteal hyperostosis type Worth, idiopathic osteosclerosis or autosomal dominant osteopetrosis type I, are clinically and radiologically very similar with an increase cortical thickness of all long bones with in many cases involvement of the skull and the mandible (Figure 2). Molecular genetic studies have shown that sclerosteosis and van Buchem disease are due to the absence of sclerostin a protein encoded by the SOST gene.[11,12] However, despite the evidence implicating sclerostin deficiency in the pathogenesis of sclerosteosis and van Buchem disease, there is little information on the mechanism by which sclerostin deficiency increases bone mass.

Figure 2. Skull x-ray of a patient with sclerosteosis; transiliac bone biopsy of a patient with sclerosteosis with thickening of the cortex and trabeculae due to increased bone formation; localization of sclerostin in osteocytes and their canaliculi in a bone biopsy from a human subject.

In several of the autosomal dominant forms of craniotubular hyperostoses missense mutations in the first propeller domain of the LRP5 protein were found.[2] Both situations are thought to result in increased Wnt signalling and, thereby, increased bone formation. There are, however, a considerable number of patients who are phenotypically very similar to patients with sclerosteosis, van Buchem disease or HBM who have none of the described genetic effects. Therefore, a more widespread mutation analysis of genes involved in Wnt signalling in such patients is expected to identify new genes involved in bone formation.
Thus, current evidence shows that Wnt canonical signalling requires LRP5/6 activity that in turn can be regulated by extracellular agonists and antagonists some of which have already been identified. Elucidation of the mechanisms involved in these interactions will not only help in the further understanding of the pathogenesis of these skeletal dysplasias and of the process of bone formation in general, but can lead to the development of therapeutic interventions aiming at correcting the remodelling imbalance of patients with osteoporosis.

1. Manolagas Sc. Birth and death of bone cells: basic regulatory mechanisms and implications for the pathogenesis and treatment of osteoporosis. Endocr Rev. 2000; 21:115-37
2. Balemans W, Van Hul W. The genetics of LRP5 in bone - A story of extremes. Endocrinology. 2007; 148: 2622-2629
3. Van Bezooijen RL et al. Sclerostin is an osteocyte-expressed negative regulator of bone formation, but not a classical BMP antagonist. J Exp Med 2004; 199:805-14
4. Poole KES et al. Sclerostin is a delayed secreted product of osteocytes that inhibits bone formation. FASEB J 2005; 19:1842-4
5. Van Bezooijen RL et al. Wnt but not BMP signalling is involved in the inhibitory action of sclerostin on BMPstimulated bone formation. J Bone Miner Res 2007; 22:19-28
6. Balemans W et al. A novel LRP5 missense mutation in a patient with a high bone mass phenotype results in decreased DKK1-mediated inhibition of Wnt signalling. Journal of Bone and mineral research 2007; 22(5): 708-716
7. Ferrari S, Deutsch S, Antonarakis SE. Pathogenic mutations and polymorphisms in the lipoprotein receptor-related protein 5 (LRP5) reveal a new biological pathway for the control of bone mass [review]. Current Opin Lipidol 2005; 16:207-214
8. Kwee M et al. An autosomal dominant high bone mass phenotype in association with craniosynostosis in an extended family is caused by an LRP5 missense mutation. J Bone Miner Res 2005; 20:1254-60
9. Balemans W et al. A generalized skeletal hyperostosis in two siblings caused by a novel mutation in the SOST gene. Bone 2005; 36:943-7
10. Van Bezooijen RL et al. SOST/Sclerostin, an osteocyte-derived negative regulator of bone formation. Cytokine Growth Factor Rev 2005; 16:319-327
11. Balemans W et al. Increased bone density in sclerosteosis is due to the deficiency of a novel secreted protein (SOST). Hum Mol Genet 2001; 10:537-43
12. Balemans W et al. Identification of a 52 kb deletion downstream of the SOST gene in patients with van Buchem disease. J Med Genet 2002; 39:91-7

Timing of work packages and their components

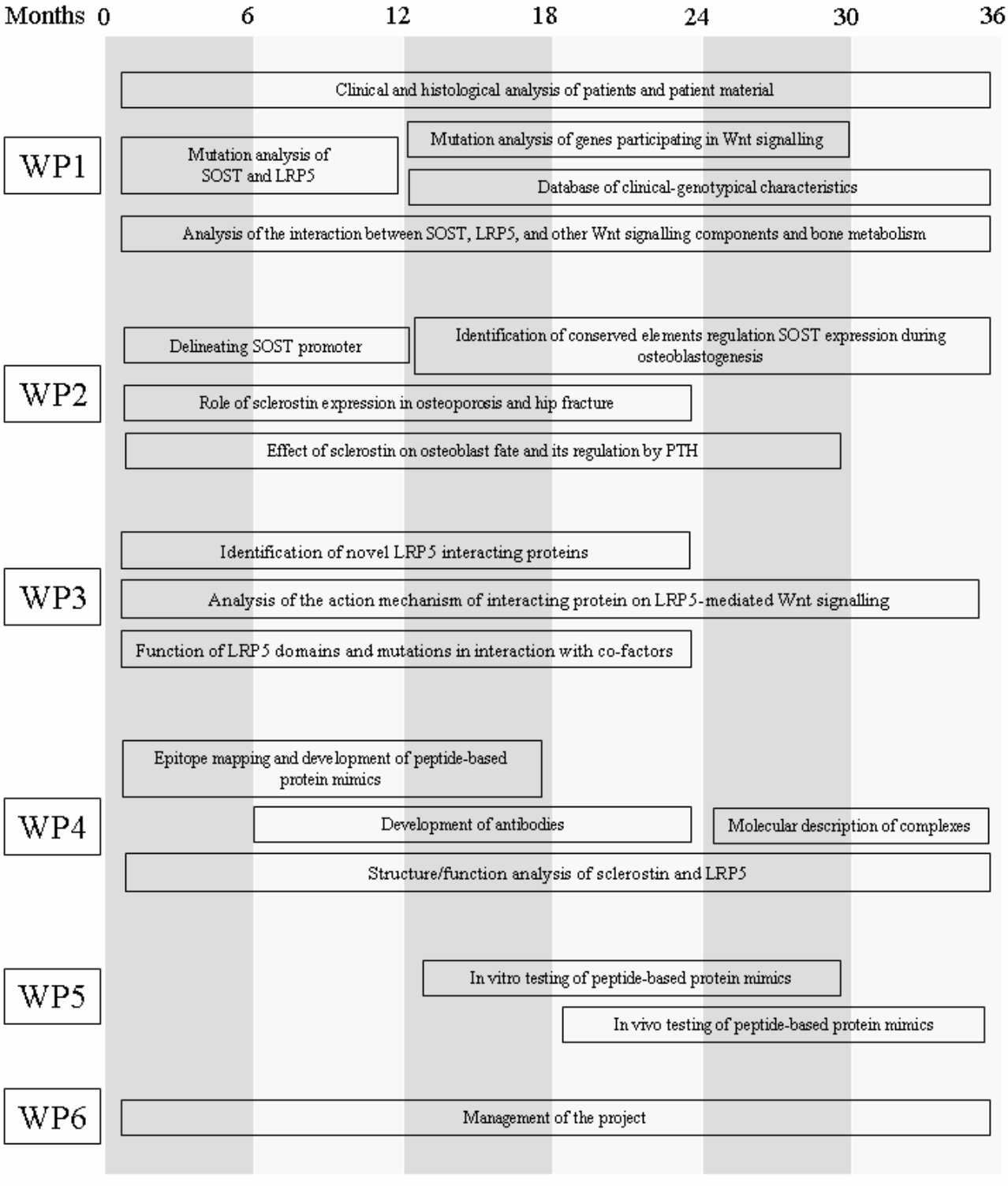

Figure 3. Timetable of TALOS

Description of the main S&T results/foregrounds

Work Package 1: Genotype-phenotype characterization of SOST, LRP5 and Wnt signaling.

Objectives:

- To identify and quantify the characteristics of bone metabolism and the genetic defects of patients with craniotubular hyperostosis, especially sclerosteosis and van Buchem disease, in order to develop a putative phenotype-genotype correlation.
- To determine the mechanism by which sclerostin deficiency increases bone mass in vivo.
- To determine how genetic variations in SOST, LRP5 and the Wnt signaling pathway modify bone architecture, remodeling and osteocyte function.

Clinical, biochemical, radiological and histological studies of sclerosteosis and van Buchem disease.

We conducted a study in a cohort of patients with sclerosteosis and their relatives who were heterozygote carriers of the SOST mutation, with the following specific aims: first, to determine how the lack of sclerostin affects parameters of bone turnover in patients with sclerosteosis, and second to assess whether sclerostin synthesis is decreased in carriers of the SOST mutation and if so, to which extent this would affect their phenotype and rate of bone turnover. Nineteen, of the 32 known, South African patients with sclerosteosis and 30 mostly first degree relatives living within a 250 km radius from Johannesburg were invited to participate in our study. The diagnosis of sclerosteosis was confirmed in all 19 patients studied by DNA analysis, on the basis of the demonstration of a C69T substitution in both alleles of the SOST gene. Of the 30 relatives, 26 were heterozygous carriers of the C69T mutation and were included in the analysis. At the time of the study 3 of the 19 patients had symptoms related to increased intracranial pressure while 13 of the remaining 16 patients had undergone decompressive surgery. The majority of patients (89%) had experienced recurrent episodes of facial palsy, usually occurring before the age of 4 years. Hearing loss was present in all cases, had been recognized in early childhood and progressed into adulthood. Other complaints associated with cranial nerves compression were decreased sensation of the face (trigeminal nerve) in two cases, and a visual field defect in one eye in one patient (optic nerve). None of the patients reported to have sustained a bone fracture. Overview of the medical history of the whole group provided insight into the natural history of the disorder. Disease manifestations first appear during childhood and adolescence and progress through to the third decade of life appearing to stabilize thereafter. In the majority of patients no recurrence or progression of symptoms were observed after the age of 25 years. Patients were of tall stature (mean height z-scores above zero; difference from relatives ($p<0.001$). Syndactyly of fingers or toes was present in 52% of the cases but patients displayed other digit abnormalities, such as nail dysplasia or radial deviation of the phalanges.

None of the carriers reported to have any of the above mentioned symptoms and none had abnormal findings on clinical examination. Similar to patients, none of the studied carriers had ever sustained a fracture.

Sclerostin was undetectable in the serum of patients, but was measureable in all carriers (mean:15.5pg/ml), in whom it was significantly lower than in healthy controls (40.0pg/ml; p<0.001). P1NP levels were highest in patients (153.7ng/ml; p=0.01 vs carriers, p=0.002 vs controls), but carriers also had significantly higher P1NP levels (58.3ng/ml) than controls (37.8ng/ml; p=0.006). In patients and carriers, P1NP levels declined with age, reaching a plateau after the age of 25 years, remaining just above or below the upper limit of the normal range (figure 1.1).

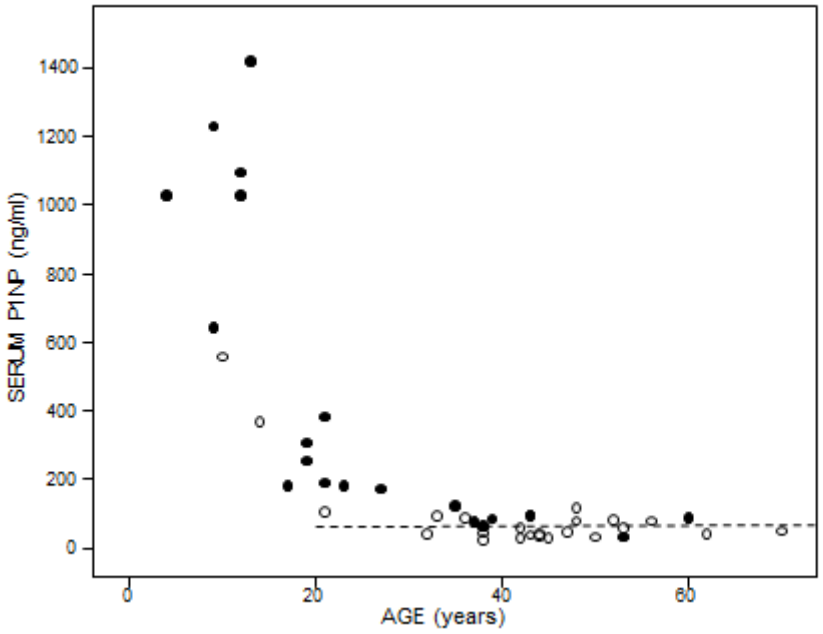

Figure1.1 *Relationship between age and serum P1NP levels in patients with sclerosteosis (closed circles) and heterozygous disease carriers (open circles). Interrupted line represents the upper limit of adult normal range.*

Serum sclerostin and P1NP were negatively correlated in carriers and age- and gender-matched controls (r= 0.40, p=0.008). These results help to explain the stabilization of the clinical complications of sclerosteosis with ageing. Mean CTX levels were well within the normal range and were not different between patients and disease-carriers after adjusting the values for age (p=0.22). Histomorphometric analysis of bone chips from patients and controls were in full agreement with the biochemical results. Bone from patients with sclerosteosis showed evidence of increased formation in that there was a higher proportion of canals with an osteoid seam compared to bone from similar sites in control subjects (sclerosteosis: 2.6 to 21.1%; controls: 1.1 to 3.7%). There was no evidence for any increase in the proportion of canals undergoing resorption (sclerosteosis: 0.6 to 3.0%; controls 0 to 0.9%). Similar to the relationship between serum P1NP and age, bone formation was highest at puberty while in the only adult patient analysed it was 2 to 3 fold greater than that of controls, while bone resorption was similar. The mineralization and material properties of bone was examined by quantitative backscattered electron imaging and Raman microspectroscopy by Drs Roschger, Paschalis and Klaushofer (Ludwig Boltzmann Institute of Osteology, Vienna). Results showed no evidence of hypermineralized bone in patients with sclerosteosis but, revealed instead, a shift towards a lower mineral content and increased heterogeneity as seen in newly formed bone. Material properties of bone from patients with sclerosteosis were also very

favorable in particular the mineral/matrix and mineral maturity/crystallinity ratios (*Manuscript in preparation*). Thus, the bone formed in the absence of sclerostin is of excellent quality and the results are, further, consistent with the lack of any reports of bone fractures in patients with sclerosteosis and carriers of the disease. Finally, to address the question of whether the lack of sclerostin may lead to compensatory changes of other osteocytic markers, we examined the expression of DMP1, DKK1 and β-Catenin in osteocytes of these bone biopsies but no marked alterations in their expression was found. Measurements of circulating DKK1 have been also performed and results are currently analyzed.

These findings provide in vivo evidence of increased bone formation caused by the absence or decreased synthesis of sclerostin in humans. They also suggest that inhibition of sclerostin can be titrated, since the decreased sclerostin levels in disease carriers, did not elevate bone formation to the same extent as in patients with sclerosteosis and did not lead to any of the symptoms or complications of the disease but had a positive effect on bone mass (*van Lierop et al 2011*).

In addition, clinical, biochemical and densitometric evaluation of 14 patients with van Buchem disease and 33 first degree relatives was completed and results are currently analyzed. We showed for the first time that sclerostin expression is absent or strongly decreased in osteocytes and cementocytes of patients with van Buchem disease suggesting that the deleted genomic non-coding region of SOST is essential for the expression of sclerostin by osteocytes. Bone histology showed excessive bone formation with no evidence of a mineralization defect or abnormalities of bone matrix (Figure 1.2, *van Bezooijen et al 2009*).

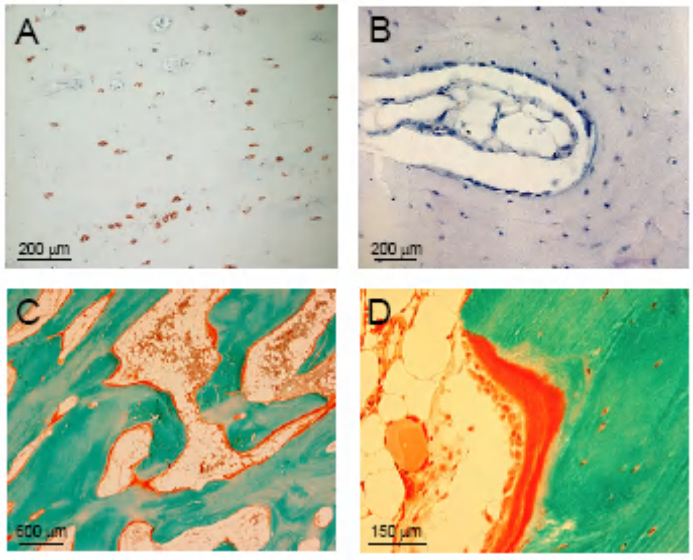

Figure 1.2. *Absence of sclerostin expression by osteocytes and increased osteoid synthesis in van Buchem disease. (A) Positive sclerostin exoression by osteocytes in cortical bone from a 12-year healthy girl. (B) Absence of sclerostin expression in a bone specimen from a 15-year old girl with van Buchem disease. (C) Goldner stain from the same patient showing increased osteoid surfaces and lamellar structure. (D) High power magnification showing active cuboid osteoblasts and normal number of lamellae.*

Conversely, glucocorticoid treatment of a patient with van Buchem disease arrested bone formation and alleviated symptoms of increased intracranial pressure, providing for the first

time a therapeutic option for these patients other than dangerous surgery (*van Lierop et al 2010*).

In these studies we used and fully characterized (in collaboration with beneficiaries 5 and 8) a very sensitive assay for the measurement of sclerostin in serum. Due to the specificity of this assay for sclerostin as evidenced by the results of the studies in sclerosteosis we have extended our original plan and we investigated further the role of sclerostin in bone metabolism in other conditions. These include endogenous and exogenous glucocorticoid excess (prednisone treatment, Cushing's disease), bone disorders characterized by a wide range of bone turnover (Paget's disease, bone metastases from prostate cancer) and pharmacological interventions leading to increased bone fragility (thiazolidines in diabetes mellitus type 2). In addition, in collaboration with beneficiary 6, we investigated circulating sclerostin levels using 2 different immunological assays recognizing different epitopes in 190 healthy subjects (100 women and 90 men) aged 65±1 years, belonging to a cohort of young retired workers (inclusion criteria : age between 63 and 67 years). Such a well homogenous group allowed us to minimize the influence of age on the results. The relation between circulating sclerostin levels and whole body, spine and proximal femur bone mineral content/areal density (as meassured by DXA), micro-structure (evaluated by HR-pQCT, Scanco Xtrem CT) at weight-bearing (distal tibia) and non-weight-bearing (distal radius) sites, and turnover markers was assessed (all these results are currently analyzed and will be submitted for publication, the article on diabetes mellitus type 2 is in press).

Mutation analysis

DNA from a set of patients with craniotubular hyperostoses were analysed for mutations in the SOST or the first propeller domain of LRP5. First, we reported one familial and one isolated case of Brazilian origin with the clinical and molecular diagnosis of sclerosteosis. The radiological and clinical features were described, and the diagnosis of sclerosteosis was confirmed in both cases by mutation analysis of the SOST gene showing a homozygous nonsense mutation (Trp124X) in the two patients. We reported this mutation previously in other sclerosteosis patients from a consanguineous Brazilian family. Interestingly, all three families were from the same state in Brazil, but they denied familial relationship. These patients confirm the clinical picture as found in other cases with a loss of function mutation in the SOST gene. (*Kim et al. 2008*).

Next we identified the first missense mutation in the SOST gene. In a small Turkish family with sclerosteosis, we identified a missense mutation (c.499T>C; p.Cys167Arg) in exon 2 of the SOST gene (Figure 1.3). This type of mutation has not been previously reported and using different functional approaches, we showed that it has a devastating effect on the biological function of sclerostin. The affected cysteine is the last cysteine residue of the cystine-knot motif and loss of this residue leads to retention of the mutant protein in the ER, possibly as a consequence of impaired folding. Together with a significant reduced ability to bind to LRP5 and inhibit Wnt signaling, the p.Cys167Arg mutation leads to a complete loss of function of sclerostin and thus to the characteristic sclerosteosis phenotype. (*Piters et al. 2010*).

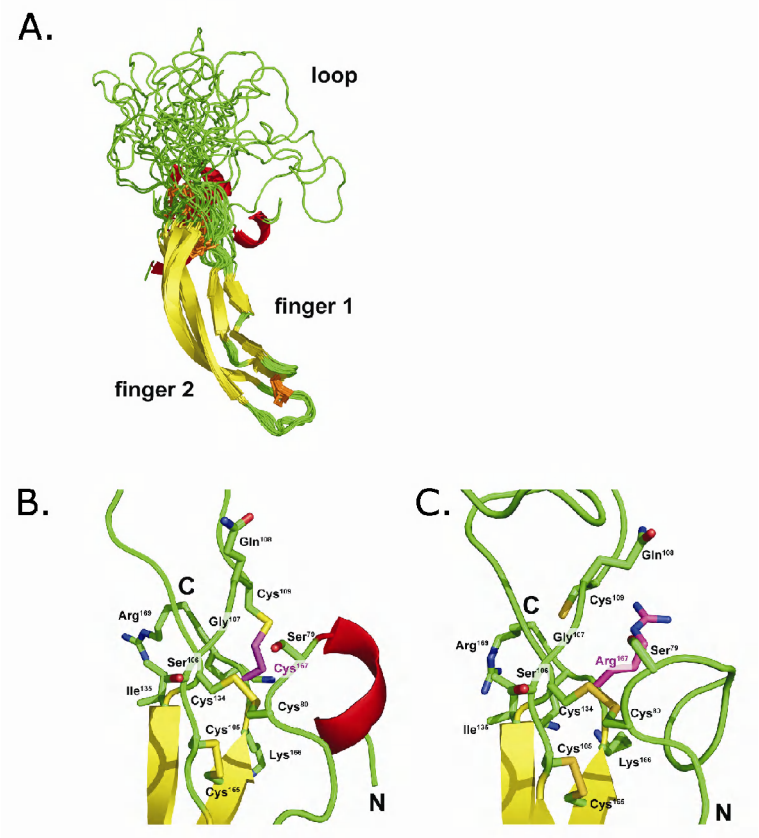

Figure 1.3. *Effect of the mutated cysteine 167 to arginie in the NMR structure of sclerostin. (A) Mouse sclerostin. (B) Details of the cystine-knot of sclerostin. (C) Same region for MT mouse sclerostin variant. Mutating cysteine 167 to arginine disrupts the outer disulphide bone present in the cystine-knot motif.*

Next, we described a patient who presented with a clinical picture of Autosomal Dominant Osteopetrosis type I (ADO I), in whom we could identify the first deletion in the LRP5 gene causing increased bone mass. This mutation caused the in-frame deletion of two amino acids in the fourth blade of the first propeller of the protein, namely the highly conserved glycine at position 171 and the following glutamate residue. In vitro studies suggested that the pathogenic effect of this novel mutation could be due to a decreased inhibition of Wnt signalling by the antagonistic proteins sclerostin and Dickkopf-1, encoded respectively by the SOST and DKK1 genes, in the presence of mutated LRP5. Our results highlight an increasing molecular heterogeneity in LRP5-related bone diseases. (*Pangrazio et al. 2011*).

Next, we screened this set of patients for other genes associated with the Wnt-signalling pathway including the Glypicans, DKK1 and 4 and SFRP1 and 4. The most interesting results were obtained for LRP4 (low density lipoprotein-related protein 4) as it was identified in tandem affinity purification proteomics screens as a sclerostin interaction partner. Biochemical assays with recombinant proteins confirmed that sclerostin LRP4 interaction is direct. Interestingly, in vitro overexpression and RNAi-mediated knockdown experiments revealed that LRP4 specifically facilitates the previously described inhibitory action of sclerostin on Wnt1/β-catenin signaling. We found the extracellular β-propeller structured domain of LRP4 to be required for this sclerostin facilitator activity. Immunohistochemistry demonstrated that LRP4 protein is present in human and rodent osteoblasts and osteocytes, both presumed target cells of sclerostin action. Silencing of LRP4 by lentivirus-mediated shRNA delivery blocked sclerostin inhibitory action on in vitro bone mineralization. Notably,

we identified two mutations in LRP4 (R1170W and W1186S) in patients suffering from bone overgrowth. We found that these mutations impair LRP4 interaction with sclerostin and its concomitant sclerostin facilitator effect. Together these data indicate that the interaction of sclerostin with LRP4 is required to mediate the inhibitory function of sclerostin on bone formation, thus identifying a novel role for LRP4 in bone. (*Leupin et al. 2011*). Also the conserved sequence in the region deleted in van Buchem patients that was shown to drive the osteocytic expression of this gene was sequenced in this set of patients but no mutations were found.

We also looked whether there is an effect of DKK1 polymorphisms on bone mineral density (BMD), hip geometry, and bone turnover. DKK1 is a secreted protein that binds to LRP5/6 receptors and inhibits canonical Wnt signaling. Using HapMap, we selected three SNPs covering the genetic variation in a 13.53-kb region comprising DKK1. The Odense Androgen Study is a population-based study comprising 783 Caucasian men aged 20-29 years. BMD and hip structural parameters were available for study. Bone turnover markers were used as a secondary end point. All analyses were repeated after adjusting for covariables and in subgroups according to physical activity. We found no significant association between DKK1 and BMD or markers of bone turnover; however, a significant association (P = 0.012) was found for rs1569198 with hip axis length (HAL), independent of BMD and height. Moreover, the association seemed to be driven by the non-sedentary subgroup (P = 0.004). Haplotype analysis further confirmed the association of rs1569198 with HAL. Furthermore, we obtained indications for interaction between DKK1 and LRP5 genotypes for different hip geometry parameters. As almost all variance within the DKK1 gene was covered, we conclude that common variation in this gene does not markedly influence BMD or bone turnover markers in young men. In this population, however, a common SNP in DKK1 does have a significant effect on HAL, implying a possible effect on hip fracture risk in the general population. This finding could be of interest but needs replication in independent populations (*Piters et al. 2010*).

Determination of the effects of SOST and LRP5 genetic variations on bone mass and architecture during growth and interaction with physical activity

SNPs in both LRP5 (LDL receptor-related protein 5) and SOST (sclerostin) genes have been consistently associated with BMD in multiple single and genome-wide association studies (GWAS). However their eventual association with microstructural determinants of trabecular and cortical bone strength are unknown. We assessed cortical and trabecular microstructure and vBMD, as well as bone geometry (cross-sectional area, CSA) at distal tibia and radius by high-resolution (HR)-pQCT (Scanco, Switzerland) in 273 pre- and post-menopausal women (mean age ±SD, 47.7 ±4.5 yrs, n=77 post-menopausal), 125 of their daughters (mean age ±SD, 20.4 ±0.6 yrs) and 176 of their sons (mean age ±SD, 15.2 ±0.5 yrs). Heritability (h2) of bone microstructural parameters was estimated by linear regressions within 101 mother-daughter (M-D) and 161 mother-son (M-S) pairs. The following SNPs were determined by pyrosequencing: LRP5 rs4988321 (G>A ; protein sequence Val667Met) and rs3736228 (C>T; protein sequence Ala1330Val) as previously reported *(Ferrari et al, Am J Hum Genet 2004, 74:866-75);* Sost rs=1513670 (G>A) and rs1983490 (C>T) (*Spector, Ann Intern med 2009, 151:528-37)*, and rs10534024 (GGA>del) (*Uitterlinden et al, Am J Hum Genet 2004, 75: 1032-45)*. Association analyses were performed separately in pre-/post-menopausal women (mothers) on one side, and young males and females (offspring) on the other side, by 2F-ANOVA including genotypes and menopausal status (pre-/post-) in the mothers, respectively

sex (m/f) in the offspring. Two groups LRP5 genotypes and 3-groups SOST genotypes were used for these analyses, accounting for the rare occurrence of LRP5 c.2047AA and c.4037TT genotypes (which were therefore grouped with AG and TC genotypes, respectively) (Table 1.1). Associations were confirmed by multiple regressions adjusting for age, weight, height and energy expenditure (as evaluated from physical activity questionnaires), sex and pubertal stage in the young, years since menopause (YSM) and smoking (No of UPA) in the pre-/post-menopausal women, and eventually for hip aBMD, the latter in order to test the specific contribution of LRP5 and SOST genotypes to bone microstructure.

Heritability was highest for bone geometry (CSA) in M-D (96%), followed by trabecular (Tb) vBMD (65%), cortical thickness (CtTh, 62%), and Tb number and thickness (TbN, 52%, TbTh 49%) (p=0.0001 to 0.01), whereas cortical vBMD was not significantly inherited. Similar findings were obtained in M-S pairs. After adjusting for weight, height, age, pubertal stage, YSM, HRT use, and FN BMD, heritability estimates for these parameters ranged between 30% and 58%, thereby establishing evidence that genes exert additive effects on bone microstructure which are partially independent of aBMD.

Table 1.1. No of subjects per genotypic group

SNPS Genotypes	Pre-/post-menopausal women n=273	Young males and females n= 301
LRP5 rs4988321		
GG	232 (87%)	263 (89%)
GA+AA	34 (13%)	31 (11%)
LRP5 rs3736228		
CC	190 (71%)	223 (76%)
GT+TT	76 (29%)	71 (24%)
SOST rs=1513670		
GG	77 (33%)	111 (38%)
GA	121 (52%)	142 (49%)
AA	35 (15%)	39 (13%)
SOST rs1983490		
CC	105 (45%)	122 (42%)
CT	98 (42%)	138 (47%)
TT	30 (13%)	33 (11%)
SOST rs10534024		
GGA/GGA	38 (16%)	44 (15%)

GGA/del	124 (53%)	142 (48%)
Del/del	72 (31%)	107 (37%)

In total, 560 subjects had complete LRP5 genotypes, and 527 complete SOST genotypes. In pre- and post-menopausal women, LRP5 (CT+TT) genotypes were associated with significantly lower TbN at both tibia (p=0.006 by 2F-ANOVA) and radius (p=0.03), whereas GA+AA genotypes were associated with significantly lower TbN (p=0.026) and higher TbTh (p=0.039) at tibia only. After adjusting for multiple co-variates (see above), including hip aBMD, LRP5 T and A alleles remained significantly associated with lower TbN (p=0.0057 for both). There were other associations of borderline significance after multiple adjustments (eg. increased CtTh with T alleles, p=0.04, increased TbTh with A alleles, p=0.06, and increased trabecular spacing with both alleles, p=0.06-0.08). In contrast, LRP5 genotypes were not consistently associated with trabecular or cortical vBMD nor bone geometry (CSA). Consistent with the heritability of microstructural traits (above), similar findings were obtained in the offspring (both males and females), associations being however stronger with T than A alleles and at the tibia. Moreover, in these young subjects, both LRP5 alleles were also significantly associated with reduced bone size (CSA, p=0.0002). In summary, LRP5 genotypes were most consistently associated with trabecular number independent of age, sex and menopausal status. The stronger associations with tibia compared to radius microstructural parameters suggests an interaction of these functional LRP5 polymorphisms with weight-bearing forces on the skeleton.

In young males and females, there were virtually no associations between SOST gene polymorphisms and bone microstructure, besides a trend for rs1053402 GGA/GGA homozygotes to have higher CTh at radius (p=0.0525 by 2F-ANOVA of 3 genotypes and sex). In contrast, in pre-/post-menopausal women, several significant associations were found between trabecular traits and SOST GGA>del genotypes and G>A genotypes, but not C>T genotypes, differences between genotypes appearing most prominent after the menopause.

Thus both rs=1513670 A alleles and rs1053402 GGA alleles were associated with significantly lower trabecular vBMD (tibia: p=0.0037 and p=0.011, respectively; radius: p=0.0016 and p=0.0017, by 2F-ANOVA of 3 genotypes and menopausal status) **(**Figure 1.4**)**, and TbTh (tibia: p=0.0157 and p=0.047; radius: p=0.0013 and p=0.012), increased trabecular spacing (tibia: p=0.047 and p=0.016; radius: p=0.012 and p=0.0024), as well as greater trabecular heterogeneity (tibia: p=0.015 and p=0.006; radius: p=0.017 and p=0.0059) . At the radius, both polymorphisms were also associated with significantly reduced TbN (p=0.032 and p=0.0039). The association of rs=1513670 and rs1053402 polymorphisms with tibia vBMD and TbTh remained significant after multiple adjustments as explained above.

Figure 1.4 SOST gene polymorphisms: association with trabecular vBMD in pre-/post-menopausal women

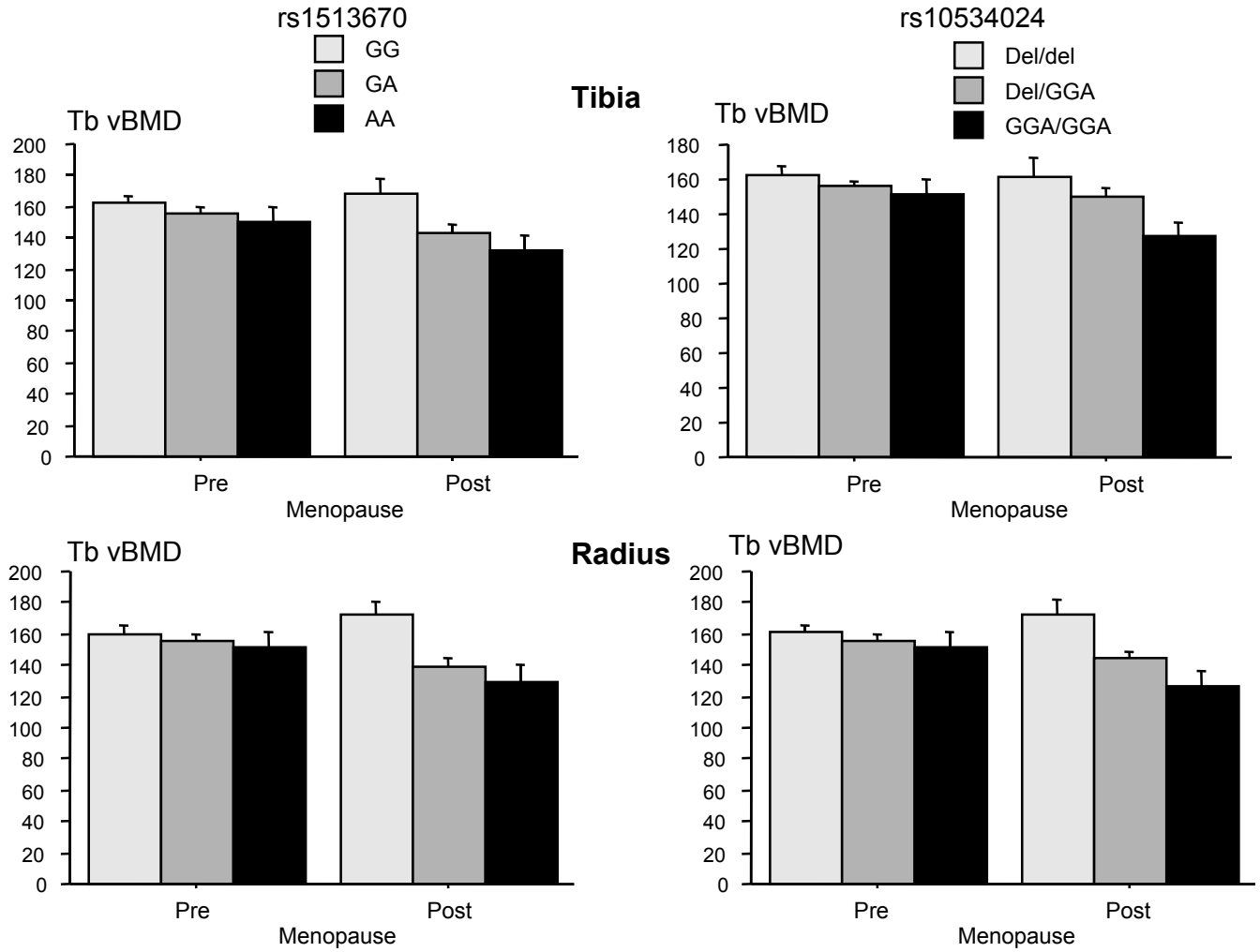

In summary, these observations indicate that SOST gene polymorphisms are associated with cancellous bone vBMD and trabecular structure at both weight-bearing and non-weight-bearing sites. Since these associations were not detected in the young but later, particularly in post-menopausal women, they suggest that SOST genotypes influence bone remodeling, particularly after estrogen-deprivation.

Analysis of the interaction between habitual loading and SOST and LRP5. Exploring the expression of LRP5-related genes in femoral neck regions experiencing different habitual loads

It has been reported that, in animal models, sclerostin expression is related to variations in mechanical loading with expression being lower in areas experiencing high loads and higher in those with low loads. In the femoral neck it is generally considered that the inferior and superior regions are exposed to the highest habitual loads while the anterior and posterior regions remain relatively neutral in their loading patterns during stance or walking. Our study indicates that while preliminary data showed that sclerostin expression was lower in the superior (% scl –ve:- 35.7 ± 12.8% (SEM) region compared to the inferior region (17.6±6.8%), once an adjustment was made for the effect of remodelling, this difference disappeared (Adjusted results: Inferior 21.6±9.8%; superior (23.8±10.5%). Sclerostin expression in the more mechanical load "neutral" cortices were midway between those of the superior and snferior cortices and less influenced by the rate of bone remodeling (Anterior:- Unadjusted: 25.4±7.4%, Adjusted: 28.6±10.4%; Posterior:- Unadjusted: 27.7±11.5%, Adjusted: 27.4±13.8%) These data do not provide support for the simple hypothesis that sclerostin expression is, in part, determined by the level of habitual load. Rather they suggest a complex relationship between load and the level of remodeling and possibly indicate that where bone remodeling is already occurring sclerostin expression may control the length of the period of bone formation rather than initiate bone formation per se. An alternative explanation to the starting hypothesis for our findings is that over preceding decades the superior cortex developed thinning as described by Mayhew et al (Lancet 2005) so that in later life mechanical loads borne by the superior and inferior cortices are in proportion to the amount of bone in these quadrants. According to this hypothesis, the differences seen in remodeling would be attributable to the superior being a tension cortex and the inferior a compression cortex. If this is the case, then osteocytic sclerostin expression may be more sensitive to tension loading than compression loading.

Assessment of the effects of genetic variability in SOST, LRP5 and Wnt signalling on bone microstructure and remodelling in hip fracture.

DNA has been extracted from the bone marrow of whole femoral neck biopsies from 116 cases of intracapsular hip fracture and sent to participant 6 to be analysed for the genetic variations in LRP5 and SOST genes. Cortical bone microstructure (cortical thickness and porosity) is being analysed in these biopsies on a regional basis (to reflect patterns of habitual loading) using the Densiscan Xtreme and Image J. Osteocyte density and viability, and bone remodelling will be analysed using standard histomorphometry. Analysis of the relationships between genetic variability and resultant changes in the cortex of the femoral neck will provide a strong basis for determining phenotype-genotype interactions at this important site of osteoporotic fracture. In the analysis of DNA from 116 (101 Females; 7 males) patients with an intracapsular hip fracture, there was no significant deviation from the Hardy Weinberg Equilibrium (HWE) and there was no effect of age or gender with respect to the

LRP5 polymorphisms (table 1.2). Cortical and cancellous microstructure is still being assessed on a case vs control basis. Analysis will be completed in 6 weeks.

Table 1.2

		Found	Expected	Chi2	P
HWE	GG	108 (101F, 7M)	107,88		
N=116	GA	7 (7F)	6,96		
	AA	1 (1F)	0,00	0.006	ns
	CC	86 (80F, 6M)	87		
	TC	28 (27F, 1M)	24,36		
	TT	2 (2F)	1,85	0,49	ns

Workpackage 2: Analysis of sclerostin expression regulation and the expression pattern in human bone biopsies.

Objectives:

- To analyze the promoter region of SOST gene in order to evaluate SOST gene expression regulation
- To reveal the expression pattern and regulation of sclerostin expression in human bone biopsies
- To evaluate bone biopsies from patients with other musculoskeletal disorders, such as osteoporosis and osteoarthritis, to better understand sclerostin function on bone metabolism.

Analysis of the SOST promoter

In order to characterize the promoter of the SOST gene the minimal promoter region was defined by making a set of constructs with different parts of the promoter region. These constructs were used in wnt luciferase reporter assays. The data indicated that the minimal promotor region contains about 300-350 bp before the startcodon. Starting from that, a next set of constructs were made with increasing 5' regions of the SOST gene. Wnt-luciferase reported assays were performed indicating that a silencer is located between 1302 and 1339 bp before the startcodon. Next, a number of constructs were generated that include different parts of the promotor region of the SOST gene but in addition also the enhancer element that

was identified from the chromosomal region deleted in patients with van Buchem disease. All these constructs were made available for testing in the osteoblastic KS483 cells.

The 6 promoter constructs (figure 2.1) were recloned into an FRT-Luciferase vector and transfected into the sequence specific (FRT) integration site of the KS483 cell line. The cell lines stably transfected with the promoter constructs were cultured under osteogenic conditions for 21 days. At several time points, the cultures were analysed for differentiation markers (alkaline phosphatase or mineralisation), luciferase expression (bioluminescence) and expression of Sost (real-time qPCR). In addition, the cell cultures were stimulated with BMP6, PTHrP and NH2-olpadronate to examine the effect of these compounds on Sost expression. During differentiation of the cultures, Sost expression increased from day 14 onwards. However, bioluminescence, which should reflect the activation of the luciferase gene by the Sost promoter constructs, increased during the first 4-7 days of differentiation and decreased thereafter. When stimulated with BMP6, an increase of luciferase expression was found, while PTHrP and NH_2-olpadronate did not show the expected decrease in luciferase expression. From these results we concluded that in these reporter cell lines luciferase expression did not correlate with Sost expression. Therefore, unfortunately we had to discontinue these experiments.

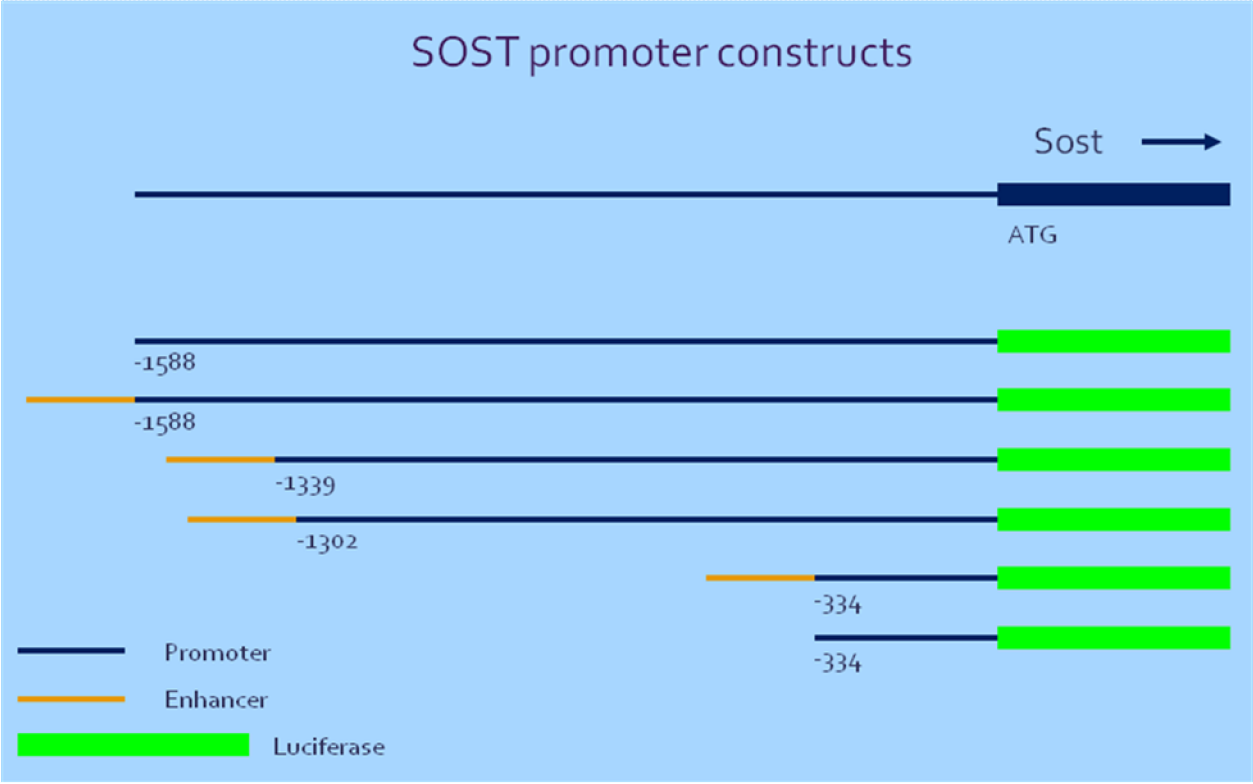

Figure 2.1

Analysis of sclerostin expression regulation and the expression pattern in human bone biopsies

Previous studies have indicated that the expression of the SOST gene is mainly restricted to bone tissue and more precisely to the osteocytes. We are generating data on the detailed expression pattern in normal and pathological bone tissue in order to understand how sclerostin regulates bone formation in vivo, because it is likely that alterations in sclerostin

expression will play an important role in osteoporosis. Furthermore, it is not possible to fully understand the effects of the SOST gene and its regulation on bone tissue homeostasis without contrasting SOST expression in diseased bone with normal bone.

Analysis of the role of sclerostin in the decreased bone formation seen in osteoporosis and hip fracture

Remodelling imbalance in the elderly femoral neck can result in thin cortices and porosity predisposing to hip fracture. By secreting sclerostin, osteocytes may inhibit Wnt signalling and reduce bone formation by osteoblasts. We hypothesised that differences in osteocytic sclerostin expression might account for differences in osteonal bone formation activity between controls and subjects with hip fracture. Using specific antibody staining, we determined the osteocytic expression of sclerostin within osteons of the femoral neck cortex in bone removed from subjects undergoing surgery for hip fracture fixation (FNF: 5M, 5F 73-87y) and controls (C: 5M, 6F 61-90y). Sclerostin expression and distances of each osteocyte

to the canal surface and cement line were assessed for all osteonal osteocytes in 636 unremodelled osteons chosen from fields (~0.5mm diameter) with at least one canal staining for alkaline phosphatase (ALP; a marker of bone formation). In adjacent sections, ALP staining was used to classify BMUs as quiescent or actively forming bone (ALP+).

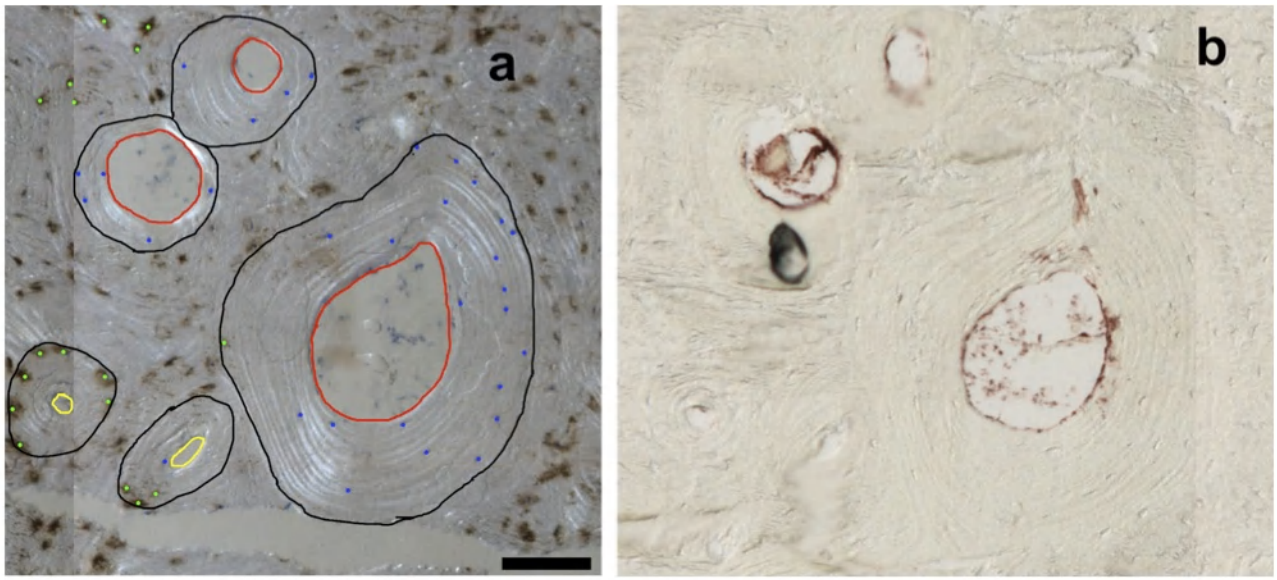

Figure 2.2. *Cortical bone images of sclerostin stained regions of the femoral neck were captured under polarised light (a). A serial section stained for alkaline phosphatase activity was captured under transmitted light (b). The initial image was colour coded using Image J to identify ALP positive and negative BMUs (red active, yellow negative), their cement lines (black lines) and canals and whether osteocytes were positive (blue) or negative (green) for sclerostin.*

The areal densities of scl- and scl+ osteocytes (number of cells per unit area) in the BMU were inversely correlated and were strong determinants of ALP status in the BMU. In controls and hip fracture cases only, sclerostin-negative osteocytes were closer to osteonal surfaces than positively stained cells. Osteon maturity (progress to closure) was strongly associated with the proportion of osteonal osteocytes expressing sclerostin and sclerostin expression was the chief determinant of ALP status. In FNF newly forming osteons that were approaching closure had a sharp reduction of ALP staining that was only partly accounted for by the

increased proportions of osteonal osteocytes staining positive for sclerostin. There was no evidence for a greater effect on ALP expression by osteocytes near the osteonal canal. In line with data from blocking antibody experiments, osteonal sclerostin appears to be a strong determinant of whether osteoblasts actively produce bone. In FNF full osteonal closure is postponed, with increased porosity, in part because the proportion of osteocytes expressing sclerostin increases sharply with osteonal maturation (*Power et al 2010*).

Figure 2.3. *Sclerostin Expression at the Fracture Site*

The non-union of bone fractures is a major clinical and economic problem consuming huge health services resources and there is great clinical interest in using anabolic therapies such as teriparatide for enhancing fracture healing. However, it is unclear as to how the cellular changes at the fracture site may regulate the speed of fracture healing. Although sclerostin mRNA is reduced in tissue taken from fracture cases (PLoS ONE 6: e16947; 2011) the location and anatomical extent of this effect relative to the fracture site is unclear. This might greatly influence the potential for anti-sclerostin antibodies to enhance fracture healing since this is likely to depend partly on the local levels of sclerostin expressed by osteocytes in the vicinity of a fracture. As well as on circulating sclerostin levels. We therefore studied femoral neck biopsies taken from patients treated by arthroplasty in the days following intra-capsular hip fracture. Each patient's date of fracture and of operation was logged and the distal stump of the femoral neck (removed to allow insertion of the prosthesis) was rapidly frozen for study using methods recently described (*Power et al 2010*).

In all biopsies (n=7), sclerostin expression was markedly reduced close to the fracture surface. The arrows indicate where the cortex has fractured. To determine if this was related to possible damage during biopsy preparation, cryostat sections were cut at right angles to the

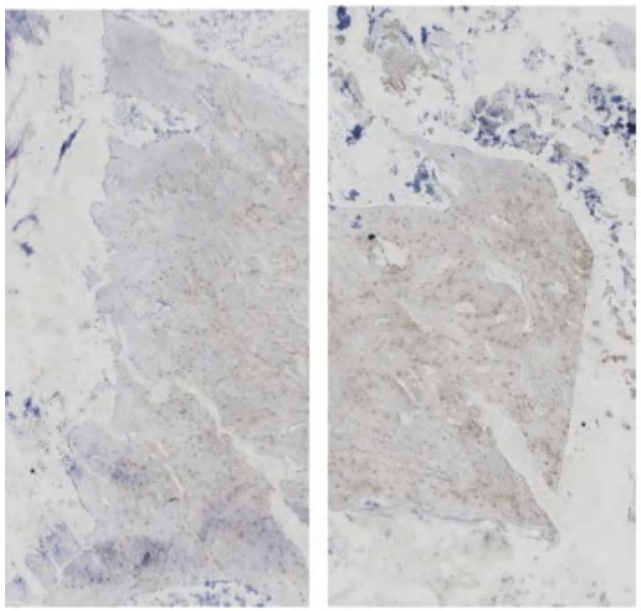

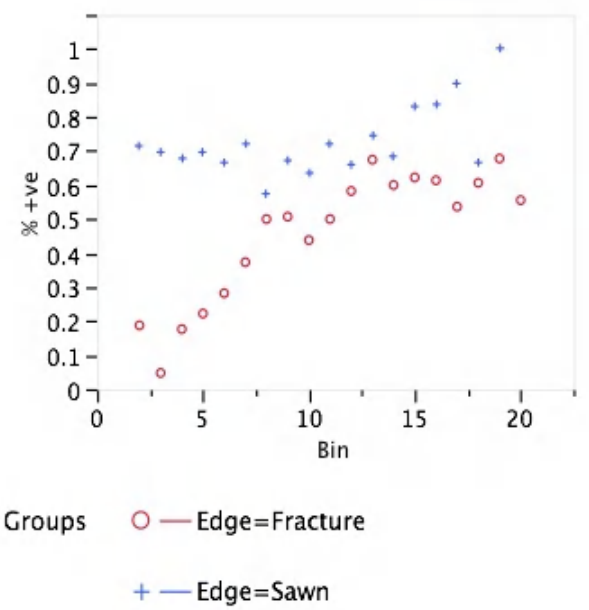

fracture plane in a way that contained both a fracture surface and sawn surface (created during arthroplasty) so that each patient acted as his/her own control.

The proportion of osteocytes positive for sclerostin (scl+ve) was measured in 0.2mm steps from fracture and sawn surfaces (figure 2.4). Sclerostin expression was reduced close to the fracture surface and slowly increased with distance from the fracture site so that at distances >1.2mm it was similar to that seen close to the sawn surfaces. There was no clear-cut loss of counterstained (sclerostin negative) osteocytes near the fracture surface and expression of key osteocyte markers (DMP-1, dkk-1) was unaffected. In conclusion, local osteocytic sclerostin expression appeared markedly reduced within 0.5mm of the fracture surface. Given that these samples were taken within a few days of the fracture occurring, this rapid loss of sclerostin expression occurs during the reactive (inflammatory) phase of fracture repair. Subsequently, this might assist recruitment and activation of osteoblasts, some from the local pre-osteoblast pool and others through re- activation of bone lining cells. However, the very localized nature of this effect makes it seem unlikely that any suppressive effect of locally produced sclerostin is blocked completely by the effects of trauma on the osteocytes immediately adjacent to the fracture surface. (*Manuscript in preparation).*

Determination of the effect of sclerostin on osteoblast fate.

Attempts to use either nick-translation or caspase 3 to determine osteoblast fate in the vicinity of osteocytic sclerostin expression have proved unsuccessful. Caspase 3 expression was rarely seen in osteoblasts and the nick-translation approach was not reproducible. The failure to detect cell death may relate to the speed at which osteoblasts undergo apoptosis resulting in only a very short window of opportunity when these methodologies will show any evidence of the process. One fate of osteoblasts is there incorporation into the bone matrix as osteocytes. However, there is little information on the osteocyte distribution within the individual osteon in cortical bone. We recently found that, in hip fracture, alkaline phosphatase is less often expressed by osteoblasts in mature osteons than predicted from the proportion of sclerostin-expressing osteocytes in communication with them. This suggested that osteonal closure slows earlier in osteoporosis than in control subjects, accounting for increased porosity, but did not reveal a mechanism. Since a limiting factor for bone formation might be osteoblast survival, we studied distributions of osteocytes, their end-form, in un-remodelled osteons in frozen sections of the femoral neck cortex. They were stained with an anti-sclerostin antibody and counter-stained with toluidine blue. Adjacent sections were stained for alkaline phosphatase (ALP). Each osteonal osteocyte was categorised as being sclerostin-positive (scl+) or negative. ImageJ was used to measure the circumference and area of each osteon and canal, while special purpose routines were used to measure the minimum distances of each osteocyte from the cement line and the canal. Canal area was strongly correlated with osteon area. Osteocytes were most dense close to the cement line and their areal density within the matrix declined up to three-fold between the cement line and the canal. Large and small osteons had similar densities of osteocytes close to the cement line, but fractured neck of femur cases had significantly lower densities of osteocytes close to the canal and higher osteocyte density close to the canal was associated with ALP expression. It is concluded that entombment of osteocytes newly drawn from the osteoblast pool into the mineralising matrix is independent of preceding bone resorption depth. As osteonal infilling proceeds, osteocyte formation declines more rapidly than matrix formation. This is consistent with but does not prove a critically declining supply of precursor osteoblasts as closure proceeds. In a statistically significant contrast between cases of hip fracture and controls,

sclerostin negative osteocytes adjacent to the canal had the statistical effect of reducing canal size in the controls but not the cases. This pointed to a likely failure of de-repressed osteonal osteoblasts to sustain bone formation through a complete remodelling cycle in osteoporosis. This failure requires further study of osteoporotic osteoblasts in situ, since it has not been traced in this investigation to their excessive suppression by osteocytic sclerostin (*manuscript accepted for publication*).

Delineation of the effect of PTH on sclerostin expression

Intermittently injected PTH 1-34, the only available bone forming therapeutic of patients with osteoporosis, down-regulates sclerostin expression. Parathyroid hormone is known to induce the activation of lining cells, but the mechanism by which it does so has remained unclear. Taken together with the evidence that sclerostin inhibits the bone forming activity, we proposed that changes in the expression of sclerostin would result in changes in the amount of bone formed per osteoblast and that changes in the expression of sclerostin during ageing and in osteoporosis is responsible for decreasing bone formation. The only biopsies available to us had already been embedded in methylmethacrylate (MMA). This process impedes access of primary and secondary antibodies so the sections have to be deplasticised prior to any immunocytochemical study. There have been technical difficulties with deplasticising bone biopsies, a process necessary for any immunocytochemical study. Efforts to achieve that also in collaboration with scientists outside the consortium (Prof P Lips, Amsterdam) were also unsuccesful. To meet our target we used an alternative approach, namely the measurement of circulating sclerostin by Beneficiary 1. In vitro and in vivo studies in animal models have recently shown that PTH inhibits the expression of the SOST gene and suggested that SOST regulation may play a role in mediating PTH action on bone. The effect, however, of PTH on slerostin production in humans is unknown. We tested the hypothesis that chronically elevated PTH concentrations decrease circulating sclerostin in humans. For this, we studied 25 patients with elevated serum PTH concentrations due to primary hyperparathyroidism (PHPT), and 49 patients with long term cure after parathyroidectomy for PHPT, who served as controls (PTX). The two groups were matched for gender, age and body weight. Serum sclerostin values were significantly lower in PHPT patients (30.5 pg/ml) compared to PTX controls (45.4 pg/ml) and serum PTH was negatively correlated with serum sclerostin ($r= -.44$; $p<0.001$). These results strongly suggest that sclerostin is involved in the action of PTH on bone in humans. The deviation from the original plan, underlying the diversity of expertise and the quick interactions of the participants, helped to obtain significant information on the relationship between PTH and sclerostin in humans (*van Lierop et al 2010*).

Workpackage 3: Co-factors of LRP5-mediated canonical Wnt signalling.

Objective:

- To identify and characterize co-factors of LRP 5 signaling.

Sclerostin binding and internalization

To get a better understanding of sclerostin binding and internalization we have generated a cell line (HEK-293) over-expressing LRP6-V5/HIS (Fig. 3.1A). With these cells we were able to show that over-expression of LRP6 enhances sclerostin-GFP binding and internalization (Fig. 3.1B). As a validation of the assay we added increasing amounts of sclerostin without GFP tag, and in this way we could compete for binding of the sclerostin-GFP to the LRP6

over-expressing cells (Fig. 3.1C). In previous publications it was described that Dkk1 (a classical inhibitor of the canonical WNT signalling pathway, which can also bind LRP6) uses the clathrin endocytosis pathway to internalize LRP6. With inhibitors of the clathrin- (mono-dansylcadaverine) and cavelolae-dependent endocytosis pathway (nystatin) we have shown that the sclerostin-GFP internalization is mediated by the clathrin endocytosis pathway (Fig. 3.1D). To go to a less artificial system we used KS483 cells, and also in these cells we could show sclerostin-GFP binding and internalization (Fig. 3.1E).

We have iodinated recombinant sclerostin, and have been able to show with crosslinking that sclerostin is mainly binding to LRP6 and to a lesser extend also to LRP5 (Fig. 3.2B, for expression of LRP5 and -6 see Fig. 3.2A). By knockdown of LRP6 using lentiviral shRNA's constructs (Fig. 3.2C) we have shown that most of the total binding of sclerostin is indeed mediated by LRP6 (Fig. 3.2D). LRP5 shRNA had no effect on the total binding of sclerostin to the cells (Fig. 3.2D). When we now used the shRNA LRP5 and -6 cells in the sclerostin-GFP binding and internalization assay we did not see any difference (Fig. 3.2E). This might be explained by the difference in concentration of the sclerostin that we used, for the crosslink experiments the concentration is somewhere around 25-50 ng/ml, and in the internalization experiments we use 500 ng/ml to get a decent signal. At higher concentrations it seems that sclerostin can bind others things than only LRP5 and -6. So far we have no data on what this other protein/factor might be.

Figure 1

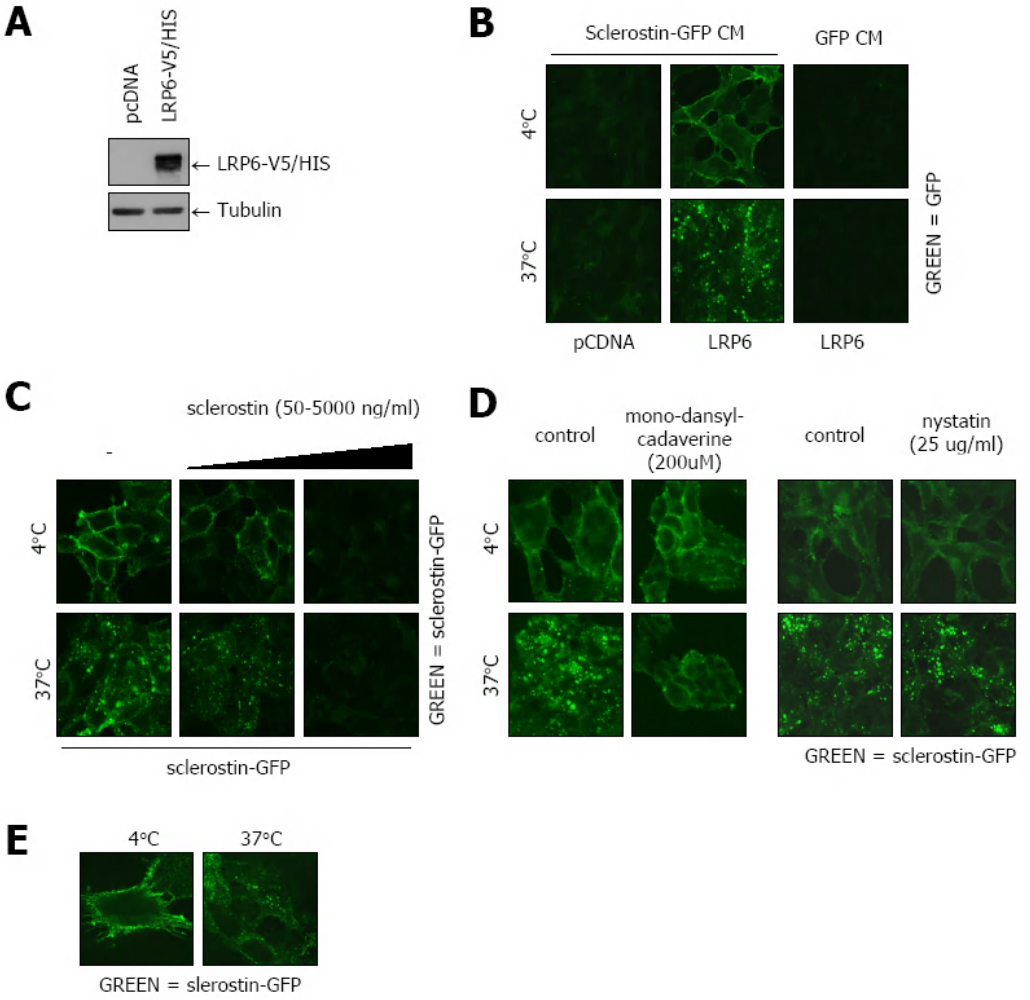

Figure 3.1

Figure 2

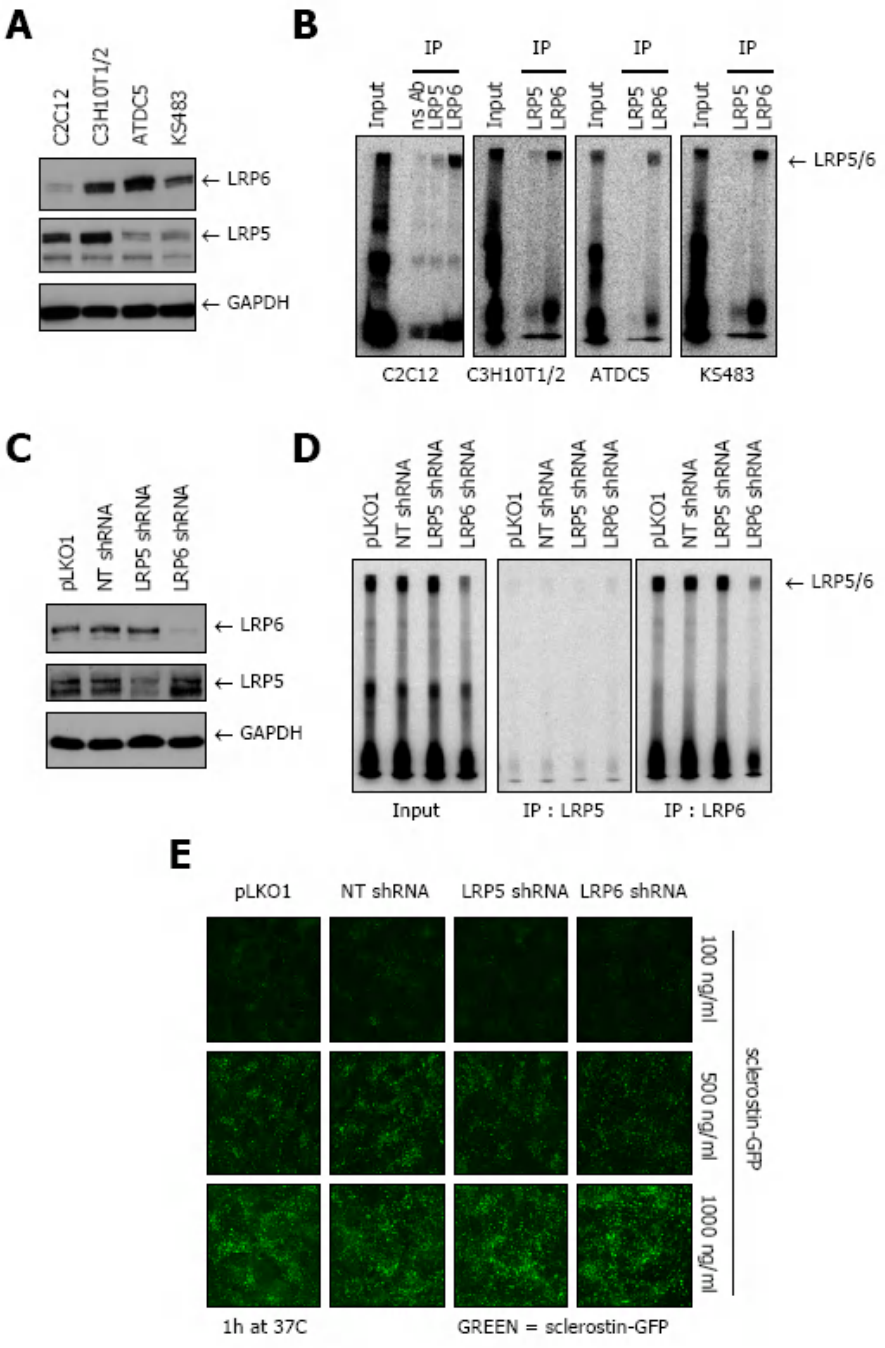

Figure 3.2

Mechanism of sclerostin inhibition of Wnt induced signalling

To get more insight into the actual mechanism of sclerostin induced inhibition of Wnt3a induced signaling we looked at one of the first steps downstream of the Wnt3a binding to

LRP5/6. It is known that Wnt3a can induce the phosphorylation of LRP5/6 on five PPSPXS motifs on the intracellular domain. In KS483 cells Wnt3a can induce the phosphorylation of serine 1490, and this can be blocked by addition of Dkk1, but not by the addition of sclerostin (Fig. 3.3A). So clearly sclerostin has a distinct mechanism of inhibition of Wnt3a induced signalling in comparison to Dkk1. In previous publications there are conflicting results that Dkk1 can induce LRP6 internalization, and in this way inhibits Wnt3a signalling. To investigate if sclerostin can induce LRP6 internalization we stimulated KS483 cells with BSA or sclerostin for different times, after this stimulation all the membrane proteins were biotinylated, then the cells were lysed and all biotinylated proteins were pulled down and a western blot was done for LRP6 (Fig. 3.3B). If sclerostin would induce LRP6 internalization there would be a reduction of LRP6 on the membrane, but this was not observed. Also, when we used Dkk1 we could not show any LRP6 internalization. As shown before sclerostin can inhibit Wnt3a induced BAT-luc activation (Fig.3.3C), but since there was no effect of sclerostin on the Wnt3a induced LRP6 phosphorylation, sclerostin might act more downstream to inhibit Wnt3a signaling. There are several ways of inducing Wnt signalling without adding Wnt ligands, like over-expression of Dvl1, Dvl2, Dvl3 or a degradation insensitive mutant of β-catenin. Also inhibition of GSK3β (by a small molecule inhibitor or LiCl) can induce Wnt signaling. We tested all these stimuli on the BAT-luc Wnt reporter, but none of these stimuli could be inhibited by sclerostin (Fig. 3.3D & 3.3E). Taken together it is still not completely clear how sclerostin can inhibit Wnt3a induced signalling, but we do know that it is not by LRP6 internalization, and that it's not by inhibiting a more downstream effector like Dvl. There are still more possibilities by which mechanism it could inhibit, like disruption of LRP6 signalling complexes (without effecting LRP6 phosphorylation).

FABs neutralize sclerostin function

Moreover, the FABs generated in workpackage 4, which were raised against human or mouse sclerostin were investigated for their possible inhibitory function on Wnt canonical signalling. By using the internalization assay, which we described in Fig.3.1, we could observe clear effect of sclersotin specific antibody (FAB-Scl) in preventing Sclerostin-GFP internalization, while the control antibody (FAB-GFP) has no such effect (Fig.3.4A). We also proved FAB-Scl could specifically prevent the binding between sclerostin and endogenous LRP5/6 (data not shown). As antagonist of WNT signalling pathway, sclerostin inhibits WNT induced reporter activity and WNT induced target genes (e.g. Axin2) expression. To identify the neutralization function of sclerostin antibody, we first performed reporter assay in mouse C2C12 cells. C2C12 cells transfected with WNT reporter were treated with control conditioned medium (CM), Wnt3a CM, or Wnt3a together with sclerostin CM and antibodies. As shown in Fig. 3.4B, FAB-Scl was able in part to rescue the sclerostin-induced inhibitory effect on Wnt3a- induced reporter activity. However, the control FAB-GFP had no such effect. Next, we examined the neutralization effect on sclerostin inhibition of Wnt-induced Axin2 expression. As shown in Fig.3.4C, Wnt3a CM induced Axin2 expression very strongly and sclerostin could partially inhibit Wnt3a-induced Axin2 expression. Notably, the sclerostin inhibition effect on Axin2 induction was partially rescued upon treatment with FAB-Scl. Taken together, the FABs is able to neutralize sclerostin-induced inhibitory effects on Wnt canonical signalling.

Figure 3

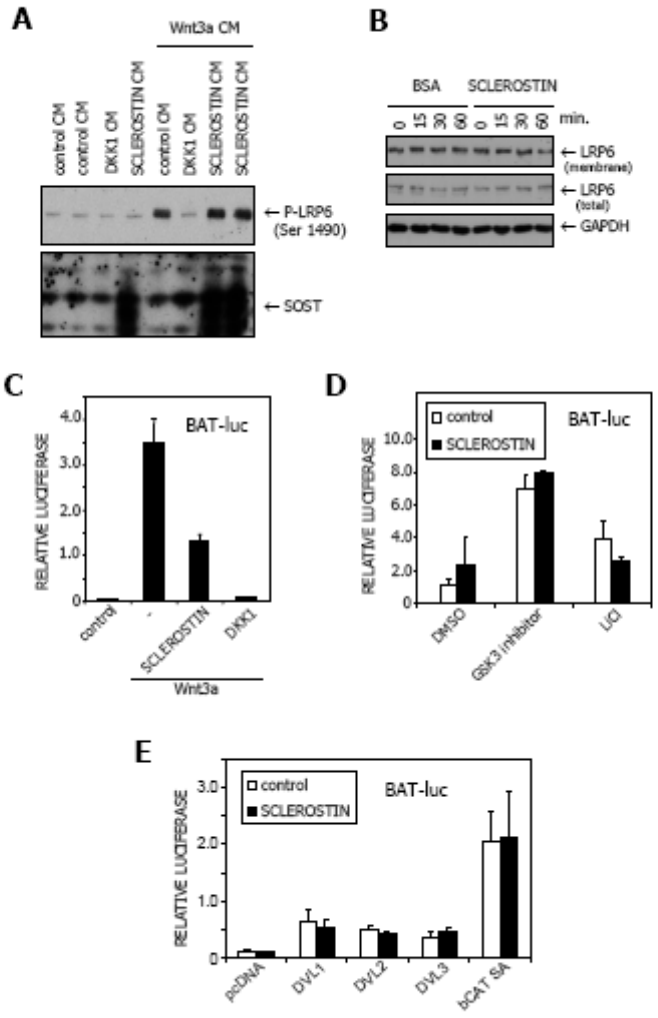

Figure 3.3

Identification of putative co-receptor

DKK1-mediated internalization of LRP5/6 is thought to involve Kremen proteins that act as co-receptors for DKK1. It is very likely that sclerostin may function besides binding LRP5/6 also requires binding of Sclerostin to specific co-receptors. Co-receptors can possibly determine target cell specificity and could be potential targets for blocking Sclerostin-mediated inhibition of WNT signalling. By blocking the binding of the co-receptor to Sclerostin or recruitment of such a co-receptor to LRP5/6 may antagonize the activity of sclerostin and, hence, increase bone mass. Thus, one of the key objectives of this workpackage is to identify putative co-receptors controlling LRP5/6 signalling, in particular those that mediate inhibition of LRP5 signalling by Sclerostin. Therefore, we have designed and synthesized a siRNA library and setup of screen for the identification of novel co-receptors regulating LRP5/6 function. For this purpose we used mouse myoblast C2C12 cells, which were transfected with a WNT canonical pathway luciferase reporter construct, internal

reference and siRNA. Luciferase activity in these transfected C2C12 cells is clearly induced upon incubation with WNT3a CM (Fig.5A), and importantly this activity was inhibited in presence of Sclerostin CM. The Dharmacon Custom ON-target plus SMARTpool library which was generated targeted 113 different mouse transmembrane proteins, including syndecans, glypicans, Kremen-1 and -2 and CD44. β-catenin, LRP5 and -6 siRNA's will be used as controls. The genes were selected based upon thoir possible role in bone formation, expression in osteoblasts, or sequence similatity to other genes previously shown to be important in regulating Wnt of other growth factors. Upon knockdown WNT target gene β-catenin, WNT induced luciferase activity is totally inhibited (Fig.3.5A). WNT induced luciferase activity was partially inhibited upon knock-down either LRP5 or LRP6 (Fig.5A). During the whole screen, 10 candidates for putative sclerostin co-receptor were identified, i.e. SDC2, FLRT1, LRP8, GP38, PLXNA1, LRP4, CAML, SEMA3A, MIC2L1 and CKLFSF3. In addition, 13 candidates for putative membrane associated WNT regulators wrre identified, i.e. AMIGO2, CDH11, SDC4, LFNG, TMEFF1, FLRT1, LRRC24, 1110007C24RIK, NTN4, LRP8, 3100001P13RIK, BC039161 and LOC381339.

Figure 4

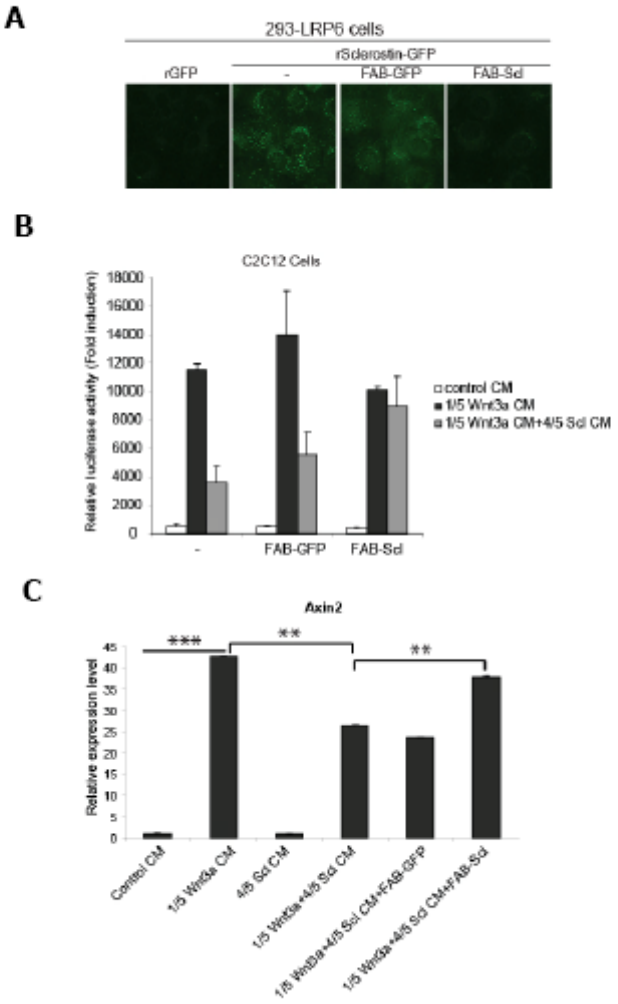

Figure 3.4

LPR8 functions as putative co-receptor of sclerostin

To further investigate the role of the putative co-receptors, affinity labelling studies were performed usining iodinated sclerostin and COS-1 cells overexpressing the genes encoding the putative candidates. In this assay, cos-1 cells were transfected with putative co-receptor candidates, or vector control or positive control, and then treated with I-labelled recombinant sclerostin proteins, followed by covalent crosslinking and subjecting the cell lysateds to SDS-PAGE and image analysis using a phosphorImager. The specific binding between LRP6 (positive controil) and LRP8 and sclerostin was clearly observed (Fig.3.5B). The specific binding between sclerostin and LRP8 was also further consolidated by immunoprecipitation. Subsequently, the role of LRP8 in sclerostin binding to and internalization of LRP5/6 will be further investigated.

LPR8 promotes WNT signalling and positively regulates Wnt induced osteoblast differentiation

Furthermore, LRP8 was identified as putative membrane associated regulator of canonical WNT signalling pathway. To find out the function of LRP8 in WNT signalling, full length LRP8 was cloned into a virus vector, and then LRP8 over-expression stable line has been made in mouse preosteoblastic KS483; the increase in LRP8 expression in the transfercted cell line was detected by real-time PCR (data not shown). To test the effect of LRP8 on WNT induced Axin2 expression. Consistent with the screen result, over-expression LRP8 clearly increased Wnt3a induced Axin2 expression (Fig.3.5C). As previously reported, WNT signaling plays important roles in osteoblast differentiation and bone formation. To check if LRP8 involved in this process, we examined LRP8 modulation on the induction of alkaline phosphatase (ALP) activity and mineralization ability. For analysis ALP activity, which is an early maker of osteoblast differentiation, we incubated confluent KS483 stable cells with the treatment of Wnt3a CM for 4 days. Histochemical staining showed that Wnt3a-induced ALP activity was highly potentiated by LRP8 over-expression (Fig.3.5D). As a (late) marker for osteogenic differentiation, we analyzed calcium deposition and formation of mineralized matrix by alizarin red S staining. LRP8 over-expression also potentiated BMP6-induced mineralization in KS483 cells (data not shown). Taken together, our results show that LRP8 promotes WNT signalling and positively regulates WNT induced osteoblast differentiation.

Identification of the Sclerostin-binding motif in LRP5

In order to identify the Sclerostin-binding motif in LRP5, Pepscan screened LRP5-derived peptides, modified to retain a secondary structure, for their ability to interact with Sclerostin. The best binder was identified and comprised the peptides *ANRRD, EDAAA*, and *DVSEEAI*. We hypothesized that these peptides might interfere with Sclerostin binding to LRP5/6. Therefore using our Sclerostin-GFP binding assay, we tested whether the isolated peptides were able to block Sclerostin binding to 293 cells overexpressing LRP5. However, incubating Sclerostin-GFP with these peptides did not affect its binding to 293-LRP5 cells (Fig. 3.6A).

All the peptides that displayed high Sclerostin-interacting capacity in the screen performed by Pepscan contained the peptide *DVSEEAI*, suggesting this is the core binding sequence. To study whether this motif of LRP5 is indeed the Sclerostin-binding motif, we generated LRP5 mutants in which the *DVSEEAI* loop was mutated. We generated the mild *EVSDDAI* mutant (*EDD*), which retains a negative charge on the same position as the wild-type LRP5, a mask *NVSQQAI* mutant (*NQQ*) in which the charge in the loop is removed, and a reverse *KVSKKAI* mutant (*KKK*) in which the negative residues are replaced by positive charged amino acids. The BAT-luciferase WNT reporter and the LRP5 mutants were co-transfected in C2C12 and the effect on WNT signalling and the inhibitory effect of Sclerostin-mediated inhibition of WNT signalling was determined. Expression of the EDD-mutant did not affect WNT3a-induced reporter activity or the inhibition hereof by Sclerostin (Fig. 6B). WNT3a-induced signalling appeared to be clearly reduced by co-transfection of the NQQ- or KKK-mutants. Nevertheless, Sclerostin still inhibited the WNT3a-induced reporter activity and the fold inhibition was similar to that in case WT or EDD LRP5 was co-transfected (Fig. 3.6B). Subsequently we determined whether the *DVSEEAI* loop mutants were able to interact with Sclerostin. FLAG-tagged Sclerostin was co-transfected with MYC-tagged LRP5 soluble LRP5 mutants and immunoprecipitation assays were performed. Sclerostin binding was to all the LRP5 mutants with no difference was observed (Fig. 3.6C). These findings indicate that

Sclerostin still binds LRP5 and is able to inhibit WNT signal transduction when the *DVSEEAI* loop is mutated, suggesting this motif is not essential for Sclerostin binding.

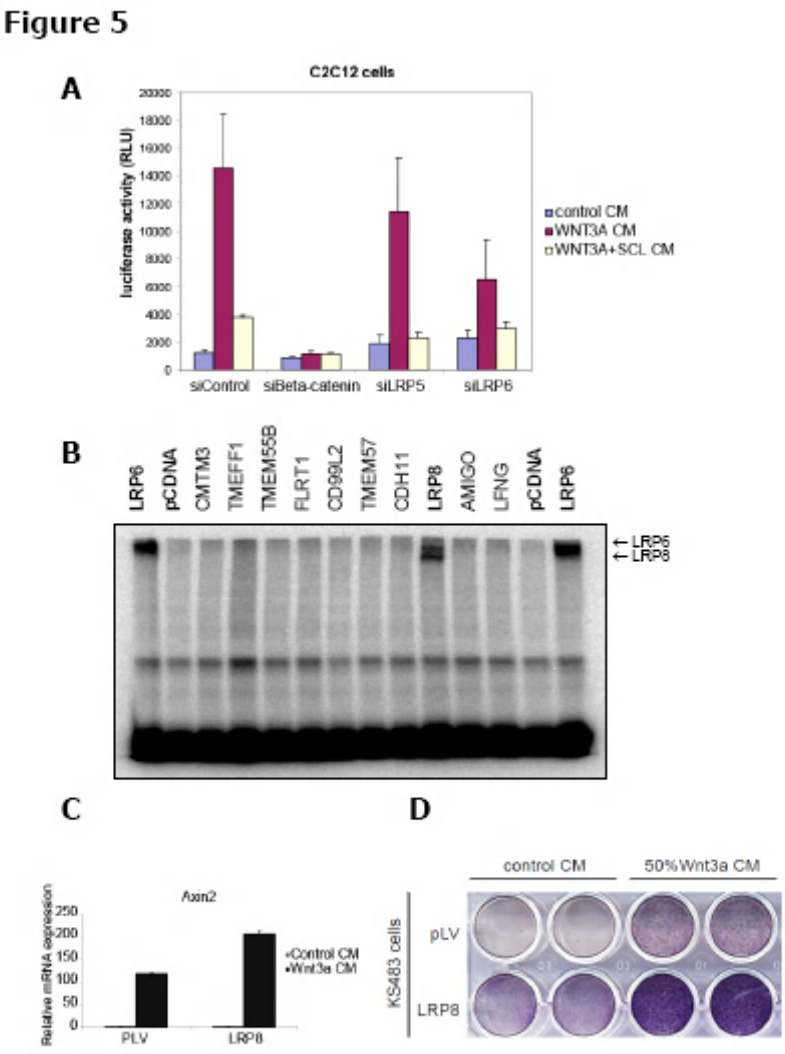

Figure 3.5

Figure 6

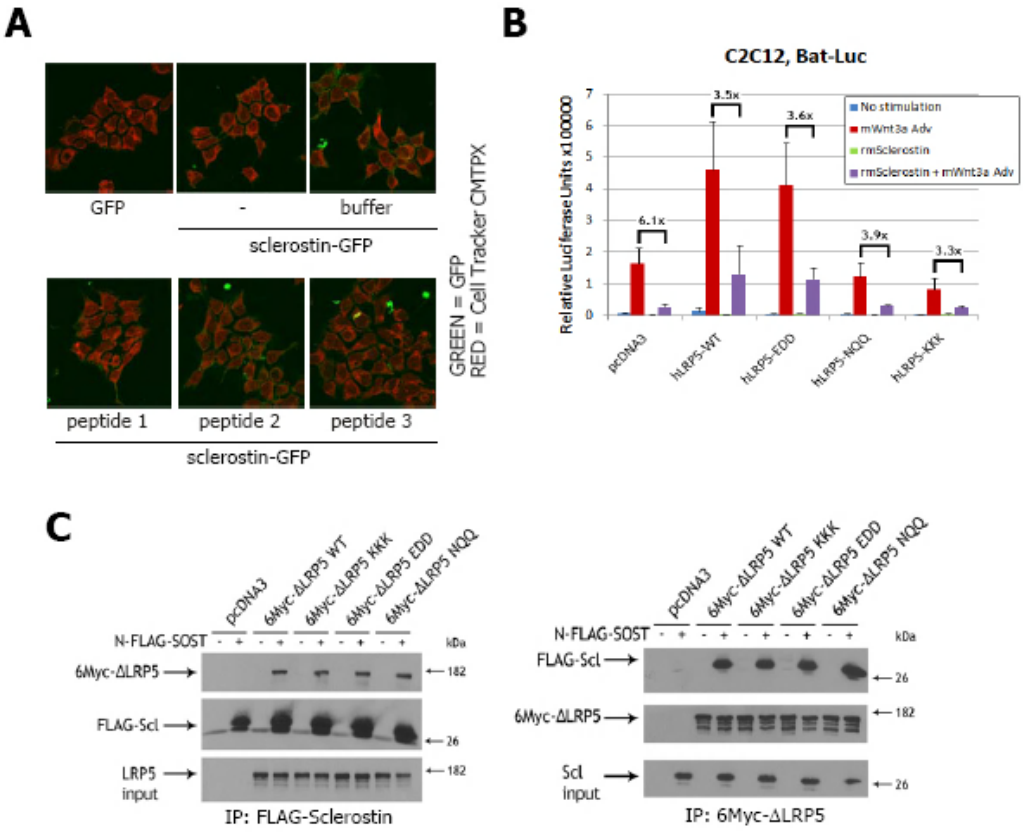

Figure 3.6

N-cadherin-LRP5 interactions in the regulation of Wnt signaling

We analysed N-cadherin and LRP5 co-localisation in vitro and in vivo. The results provided clearly indicate that N-cadherin and LRP5 co-localize in vitro and in vivo. These results demonstrate that the N-cadherin-LRP5 interaction occurs in normal osteoblasts in vitro and in vivo. These data support a functional role of N-cadherin-LRP5 interaction in the control of Wnt signalling and bone formation (*Manuscript submitted for publication*). Based on these data, we investigated whether N-cadherin-LRP5 interaction negatively controls osteoblast proliferation and survival. We showed that N-cadherin negatively controls osteoblast proliferation and survival via inhibition of autocrine/paracrine Wnt3a ligand expression and attenuation of Wnt, ERK and PI3K/Akt signalling. This provides novel mechanisms by which N-cadherin regulates osteoblast number via canonical and noncanonical Wnt signalling (*Haÿ et al 2009*).

We then performed experiments to identify the domains of interactions between N-cadherin and LRP5 in osteoblasts. We previously showed that LRP5/6 bind to N-cadherin via the last 28 AA. We showed that the physical N-cadherin-LRP5 interaction is dependent on the last 62 AA in N-cadherin. Using standard assays, we confirmed that truncation of the last 62 AA in N-cadherin was sufficient to increase the canonical Wnt/β-catenin signalling pathway, cell

proliferation, alkaline phosphatase activity and osteoblast marker gene expression in MC3T3-E1 osteoblasts (Figure 3.7).

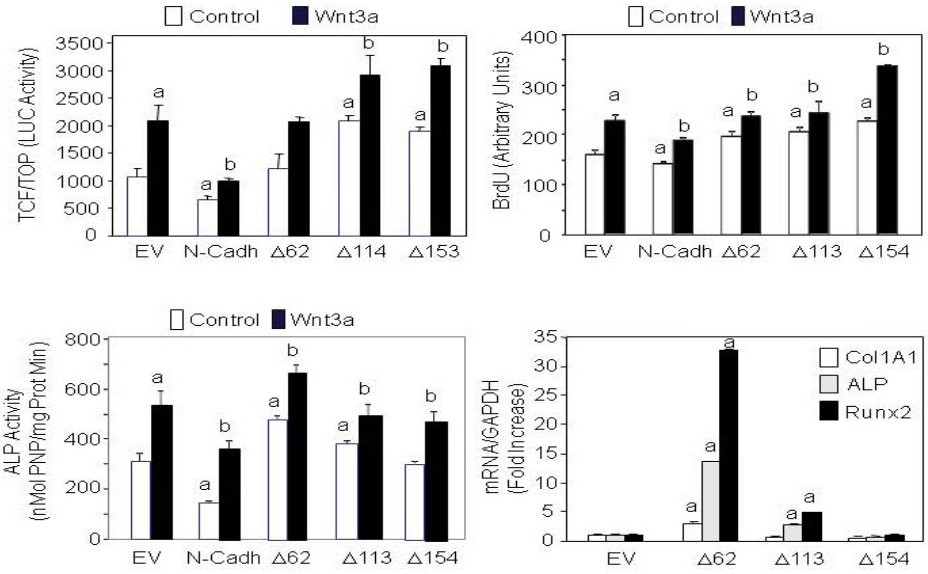

Figure 3.7.*Effects of truncated N-cadherin constructs on Wnt/□-catenin signalling, cell replication and differentiation in murine osteoblasts. Deletion of the 62 AA cytoplasmic domain in N-cadherin abrogates the negative effect of full length N-cadherin on β-catenin transcriptional activity, as shown by TCF/TOP assay. Deletion of the 62 N-cadherin domain abolishes the negative effect of full length N-cadherin on cell replication, as shown by BrdU assay. Deletion of the 62 N-cadherin domain increases alkaline phosphatase (ALP) activity, as shown by biochemical analysis) as well as osteoblast differentiation markers, as shown by RT-qPCR analysis, providing a target for modulating Wnt signaling. Data represent mean values of triplicate experiments ± s.d. (a: P<0.05 vs control; b: P<0.05 vs Wnt3a).*

These results allowed us identifying functional domains of interactions between N-cadherin and LRP5 that impact Wnt signalling and osteoblast gene expression (*Manuscript submitted for publication***).**

We also investigated whether N-cadherin may interact with LRP5/6 independently of cell-cell adhesion mediated by N-cadherin. To this goal, we transfected MC3T3-E1 osteoblasts with constructs expressing various intracellular N-cadherin domains and tested whether these domains can block cell-cell adhesion in a standard aggregation assay. As shown below (Figure 3.8), no change in cell-cell aggregation was observed in cells transfected with

intracellular N-cadherin domains, indicating that these domains impact Wnt signalling and osteoblast differentiation independently of cell-cell adhesion.

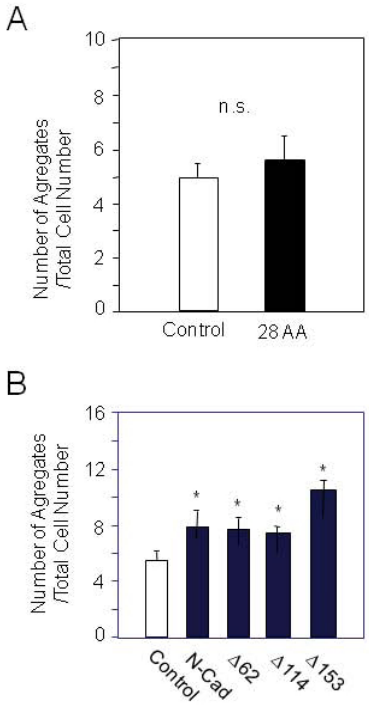

Figure 3.8. *Truncation of N-cadherin intracellular domains do not impact cell-cell aggregation in osteoblasts. Cell-cell adhesion was increased in cells transfected with full length N-cadherin, used as positive control, and in cells transfected with truncated N-cadherin intracellular domains. Data represent mean values of triplicate experiments ± s.d. (*: P<0.05 vs Control).*

In order to confirm that only the intracellular domain of N-cadherin can interact with LRP5, we transfected MC3T3-E1 cells with constructs expressing activating mutations in LRP5 (provided by beneficiary 3) and analysed changes in gene expression. As shown below, the constructs expressing activating mutations in LRP5 had no effect on LRP5 interaction with N-cadherin, showing that only the intracellular domain of N-cadherin can interact with LRP5 (Figure 3.9).

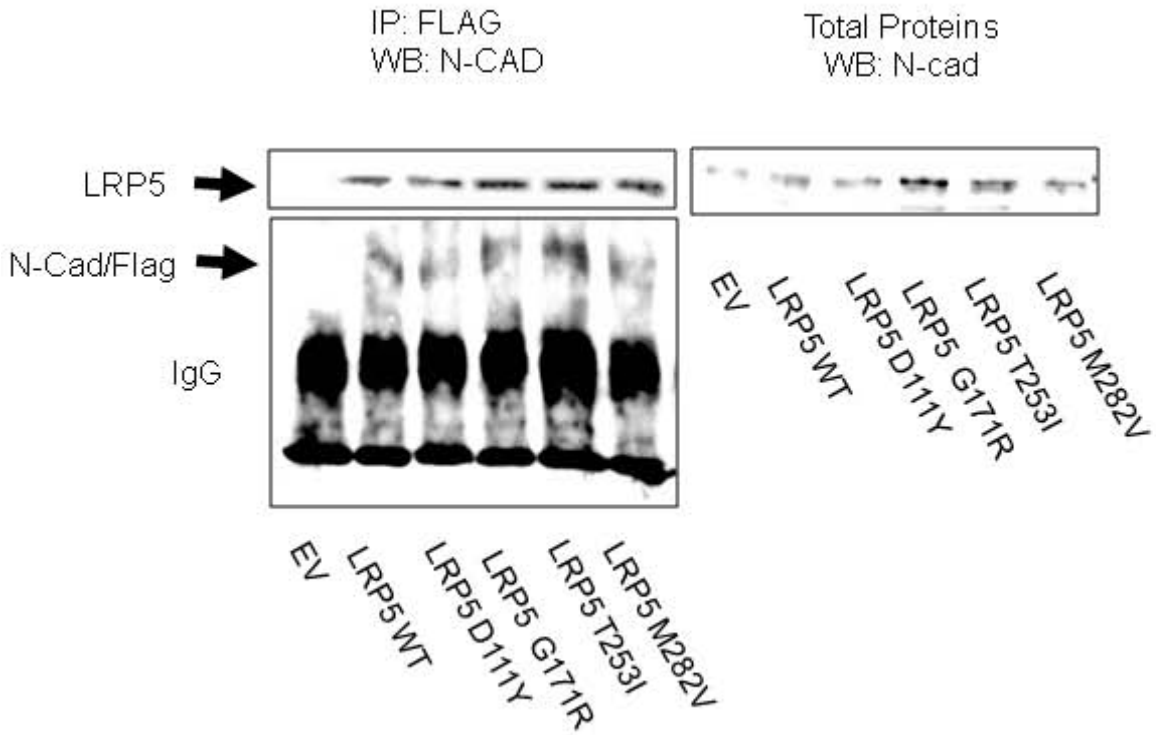

Figure 3.9. *Effects of constructs expressing activating mutations in LRP5.When MC3T3-E1 cells were transfected with various constructs that harbour activating mutations in the extracellular domain of LRP5 that activate Wnt signaling, the interaction of LRP5 with N-cadherin was preserved, showing that only the intracellular domain of N-cadherin can interact with LRP5.*

Finally, we analysed the negative impact of N-cadherin-LRP5 interactions on Wnt signalling. In particular, we identified the molecular events that are affected by LRP5/N-cadherin interactions. To this goal we analysed whether the recruitment of Frizzled (Frzd) or Kremen which are essential LRP5 co-receptors is changed in response to Wnt in osteoblasts. Our immunoprecipitation analysis showed that N-cadherin does not interact with the Wnt co-receptors Kremen or Frzd in osteoblasts (Fig. 3.10).N-cadherin increased GSK3 protein level, as expected from the reduced Wnt activity. However, N-cadherin did not directly interact with GSK3, as shown by immunoprecipitation analysis, in control cells or in osteoblasts overexpressing N-cadherin. These data indicate that N-cadherin negatively regulates Wnt signaling via its interaction with LRP5/6, and not via interaction with other Wnt-co-receptors or with GSK3, which provides clues in the molecular mechanisms by which N-cadherin-LRP5/6 interactions affect Wnt signalling in osteoblasts (*Manuscript submitted for publication).*

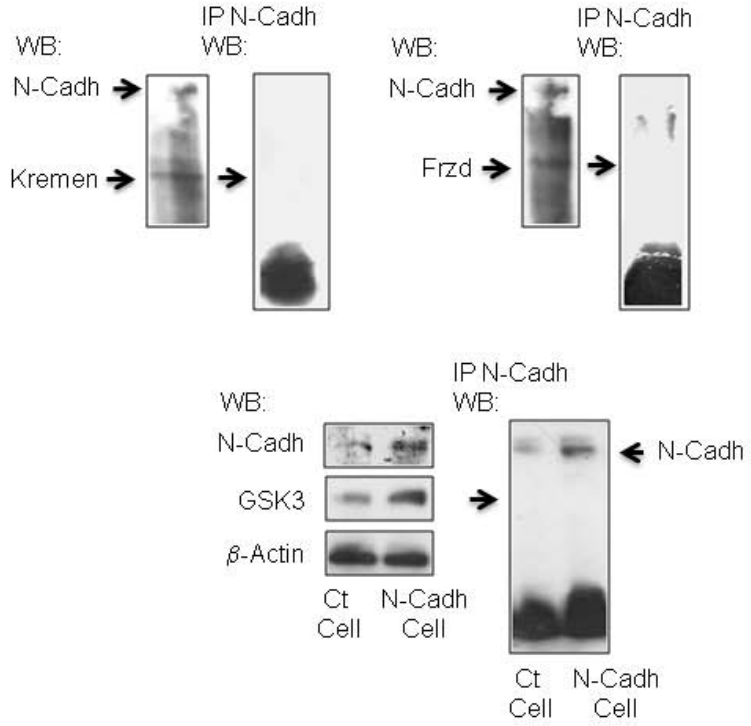

Figure 3.10 *Immunoprecipitation analysis showing that N-cadherin does not interact with the Wnt co-receptors Kremen or Frizzled (Frzd) and does not interact with GSK3 in osteoblasts. Overexpression of N-cadherin in osteoblasts increased GSK3 protein level, as expected from reduced Wnt signaling. The negative effect of N-cadherin on Wnt signaling thus results from N-cadherin-LRP5/6 interactions as there was no direct N-cadherin-GSK3 interaction, as shown by immunoprecipitation analysis.*

Mutation analysis

Mutation analysis was performed on proteins suggested to be cofactors for sclerostin including the glypicans and LRP4 as described in workpackage 1. Next we investigated six different HBM-LRP5 mutations and confirm that neither Dickkopf1 (DKK1) nor sclerostin efficiently inhibits HBM-LRP5 signaling. In addition, when coexpressed, DKK1 and sclerostin do not inhibit HBM-LRP5 mutants better than either inhibitor by itself. Also, DKK1 and sclerostin do not simultaneously bind to wild-type LRP5, and DKK1 is able to displace sclerostin from previously formed sclerostin-LRP5 complexes. In conclusion, our results indicate that DKK1 and sclerostin are independent, and not synergistic, regulators of LRP5 signaling and that the function of each is impaired by HBM-LRP5 mutations (*Balemans 2008*).

Effects of periostin on Wnt/LRP5 signaling and bone microstructure in relation to mechanical loading

In order to test the regulation of Wnt-LRP5 signaling in response to mechanical loading, we have developed and applied a protocol for axial compression of the mouse tibia in vivo by a compressive device. Two weeks of short daily stimulations significantly increase bone mass,

cortical and trabecular bone microstructure, and histomorphometrical indices of bone remodeling in wild-type mice. Our initial proposal was to test the role of a cytoplasmic signaling regulatory protein, beta-arrestin, in the Wnt-LRP5-mediated biomechanical response, by using beta-arrestin 2 KO mice. Meanwhile, we discovered that bone axial compression strongly induced the expression and production of a secreted matricellular protein, periostin, in both osteocytes, -the sclerostin-producing cell-, and the periosteum. We then turned to periostin (Postn) KO mice, in which we found that down-regulation of SOST expression and the bone anabolic response to axial compression were abolished. However, the effects of mechanical loading on new bone formation in cortical bone could be restored in Postn KO mice when concomittantly treated with Sclerostin neutralizing antibodies (a generous gift of Dr M Kneissel, Novartis , Basel, Switzerland). Taken together, these results indicated that periostin is required for SOST inhibition and thereby plays an important role in the determination of bone mass and microstructure in response to loading. (*N Bonnet et al 2009)* .

We pursued these investigations by characterizing the role of periostin on the regulation of sclerostin expression by parathyroid hormone (PTH) in vivo and in vitro in relation to PTH anabolic effects on bone. Postn and Sost mRNA levels in response to PTH (10 nM) were examined by qRT-PCR in UMR-106 osteoblast-like cells in absence or presence of Postn blocking antibodies (2 ug/ml). PTH time-dependently stimulated Postn mRNA expression in UMR106 osteoblast-like cells, while it profoundly inhibited Sost expression. In presence of periostin blocking antibodies, Sost inhibition by PTH was markedly, but not completely reduced (-33% vs -92% respectively in presence and absence of Postn Ab, p=0.004).

The effects of 6 weeks iPTH (40ug/kg) or vehicle (Veh, saline water) on bone turnover were evaluated by dynamic histomorphometry and on bone microarchitecture by micro-CT of tibia in 18 weeks-old female *Postn*$^{-/-}$ and *Postn*$^{+/+}$. In *Postn*$^{+/+}$ mice, iPTH increased bone forming indices at both periosteal and endocortical surface. In contrast, in *Postn*$^{-/-}$ mice, iPTH effects on bone forming indices were absent at periosteum and markedly lower at endocortical surfaces, while no significant interaction was observed at the trabecular surface. Consistent with these observations, iPTH significantly increased cortical bone volume and thickness at the tibial midshaft in *Postn*$^{+/+}$ mice but not in *Postn*$^{-/-}$ mice. However PTH significantly increased BV/TV and Tb. Number in both *Postn*$^{+/+}$ and *Postn*$^{-/-}$ mice.

These results confirm that PTH stimulates Postn expression in osteoblasts, which in turn is necessary for the complete inhibition of Sost expression. In absence of Postn, PTH anabolic effects on cortical bone are impaired. Moreover we demonstrated that sclerostin-blocking antibodies where not able to fully restore the anabolic response of PTH in *Postn*$^{-/-}$ mice, suggesting that periostin exerts both sclerostin-dependent, and sclerostin-independent effects on osteoblast functions (*Manuscript in preparation*)

Workpackage 4: mechanism of sclerostin-LRP5 interaction

Objectives:

- To elucidate the interactions of sclerostin with LRP5 for its inhibitory effect on bone formation.

*Peptide-based protein mimics derived from sclerostin that interact with LRP5 and from LRP5 that interact with sclerostin***:**

In order to map the binding epitopes of sclerostin and LRP5 another approach was implemented by beneficiary 8. Using their unique CLIPS technology beneficiary has prepared peptide arrays mimicking LRP5 and sclerostin. The peptides can be produced in a linear or a constrained form thereby mimicking the native fold. Since recombinant LRP5 is currently not available in sufficient amount, mapping of the sclerostin epitope on LRP5 was done first. Peptides were produced either as single loop variants or as two or three-loop CLIPS variants, totaling over 3000 immobilized peptides.

These arrays have been probed with the four human and murine recombinant sclerostin constructs provided by beneficiary 5, providing a set of three LRP5 loops that contribute most to the binding. These loops are not contiguous in the sequence, but are adjacent on a modeled LRP5 ectodomain structure. Peptides found positive for sclerostin binding have subsequently been used to model ideal binders. Putative binders have been synthesized on large scale, as well as scrambled control versions of these peptides. From these peptides subsequently linear and single and double loop CLIPS constrained forms were prepared, totaling 16 peptides, that were sent to beneficiaries 1 and 5 and are currently tested whether they can inhibit sclerostin binding to LRP5 or neutralize sclerostin activity in a Wnt-reporter assay. In addition, NMR titration studies will be performed to determine the binding epitope more precisely.

Similarly, peptides have been prepared mimicking sclerostin (beneficiary 8),. To determine the binding epitope of sclerostin for LRP5, three peptide-based sclerostin mimics were designed. One peptide (SYM117) covers finger 1 and 2 but removes/shortens the flexible loop, the second peptide resembles only the loop (PFD038) and the third peptide (tSOST) covers the entire cystine-knot domain of human sclerostin. The possible influence of the structure for sclerostin's function is also studied by providing the peptides in a conformationally restrained and a linear conformation. These peptides (restrained and relaxed forms) were sent to beneficiary 10 for raising antibodies that can be used in functional studies. Pannings on the peptides were performed and in the primary ELISA screening antibodies were tested on the respective peptide and on human These peptides have been made available to beneficiary 1b and tested for their ability to displace radio-labeled sclerostin in a cell based assay (Fig. 4.1). It was found that only the oxidized form of a peptide resembling the native fold of the loop of sclerostin was able to do so, the other constructs or other peptide versions of the loop were not able to displace sclerostin.

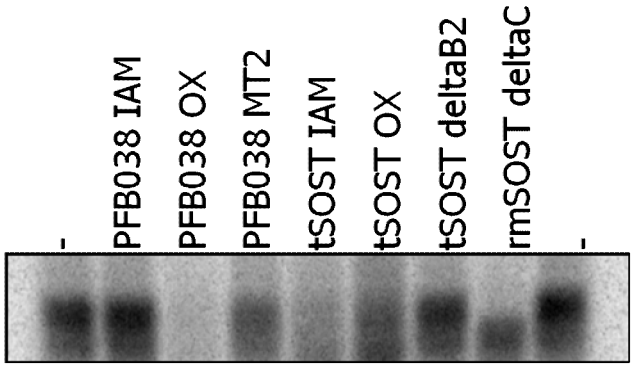

Figure 4.1: *Radiolabeled sclerostin is displaced by PFD038ox, but not by other constructs. Based on this experiment, PFD038ox was chosen to be synthesized in murine form for in vivo experiments*

Therefore, it was decided that this peptide was to be made on a larger scale, for functional testing in the laboratories of LUMC, UWUE and UNIGE. Both human and murine forms of the peptide were synthesized on 100 mg scale. The peptides have also been analyzed to test whether the loop 2 mimic alone can provide sclerostin activity, or whether the cystine-knot core motif is required for Wnt-inhibition. Whereas partner 1b could not detect any effect of the sclerostin mimics in their Wnt reporter assays as well as in their LRP5 receptor internalization assays, additional testing in the lab of partner 5 showed that the peptides 1317 (mimicking the loop of human sclerostin) and 1318 (mimicking the loop of murine sclerostin) indeed show a sclerostin-like activity, i.e. inhibit Wnt-activity in the TCF/LEF-reporter assay, although a 100-fold higher concentration compared to full-length sclerostin is required. (Fig. 4.2).

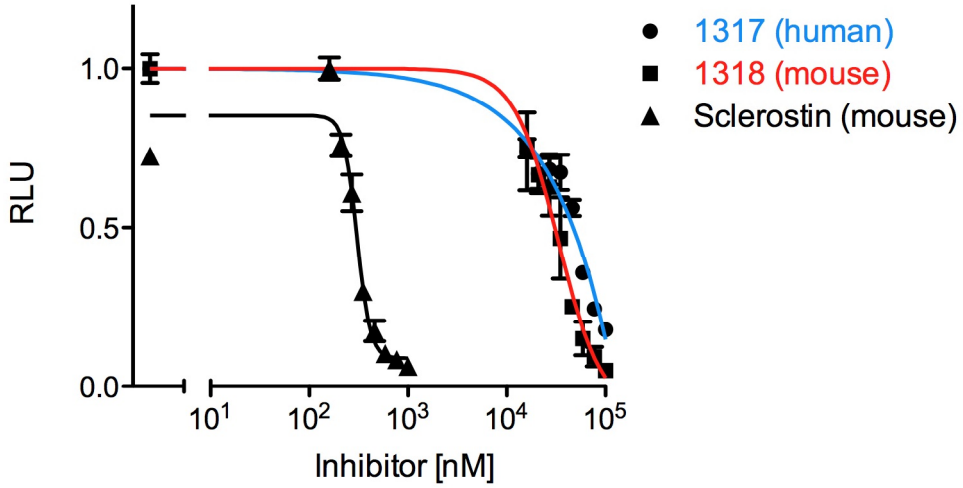

Figure 4.2: *Wnt-reporter assay measuring the dose-dependent inhibition of Wnt3a activity on HEK293T cells by sclerostin (murine) or the peptide mimicking the loop of either murine or human sclerostin.*

Molecular description of sclerostin and LRP5

At the time of our proposal neither structural data for sclerostin or its binding partner LRP5 nor a molecular mechanism how sclerostin recognizes and binds to LRP5 was available. We thus proposed to determine the structure of sclerostin and of LRP5 and the potential complex of sclerostin bound to LRP5 (deliverable 4.5, person month 36) as a part of the workpackage 4. To achieve these goals we (S. Weidauer/T. Mueller, UWUE) first generated pro- and eukaryotic expression systems for murine and human sclerostin. Highly-purified active full-length murine and human sclerostin could be derived from a baculovirus-transfected insect cell expression system. Biophysical analyses of this *Sf9*-derived sclerostin provided insights into the architecture. A proteomics approach was used to determine the disulfide-bonding network experimentally thereby confirming that sclerostin indeed harbors a cystin-knot [E1]. The analysis also showed that only the cysteine-rich region of sclerostin is structured. Proteolytically derived truncated sclerostin variants showed that the flexible N- and C-terminal regions are dispensable for inhibition of Wnt-activity [E1] (Fig. 4.3). For structure determination a truncated murine sclerostin variant with minimal flexible regions (SOST_ΔNC, residues Asn36-Arg144) was used, preparation was performed in an *E. coli*

expression system. The preparation and purification protocols allowing for large-scale preparation of sclerostin proteins were also made available to beneficiary 8 and used to generate sclerostin-mimicking peptides with complex fold.

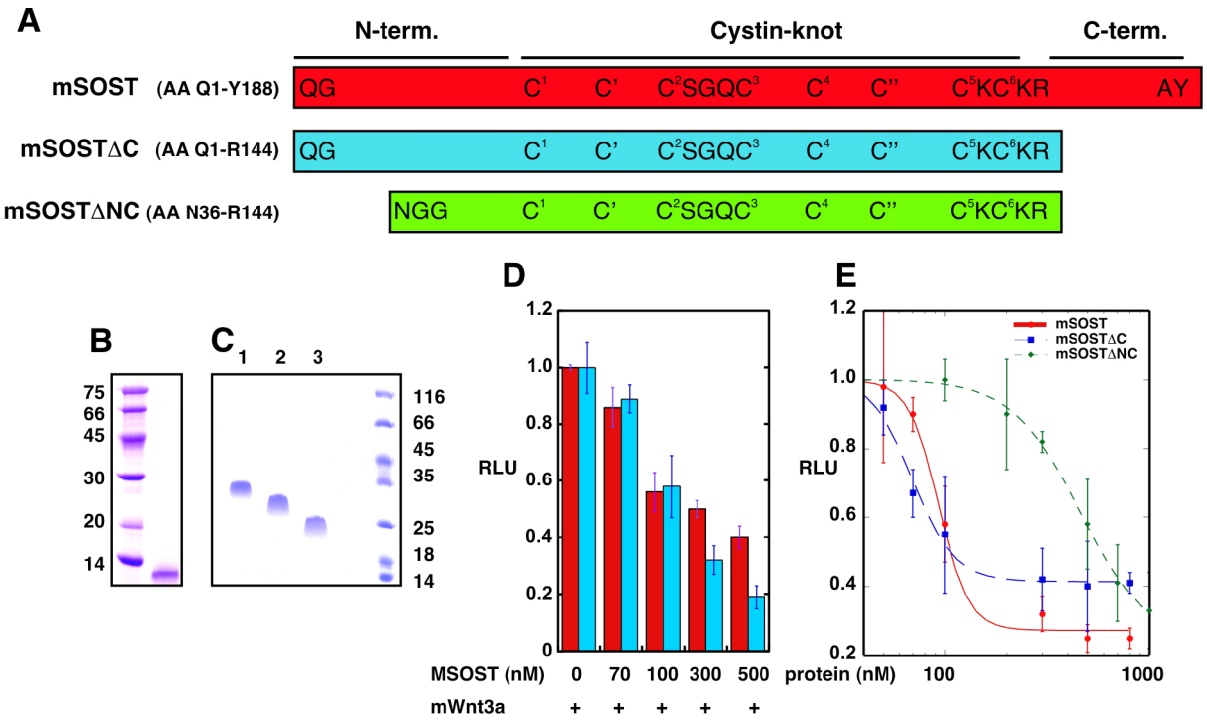

Figure 4.3: *(a) Truncation variants of murine sclerostin were expressed in E.coli. (b) SDS-PAGE analysis showed that Sf-9 derived murine sclerostin was susceptible to proteolytic cleavage when stored at 4°C over extended periods of time, however a stable degradation product of approximately 11kDa was obtained. (c) SDS-PAGE of E.coli derived full-length or truncation variants of sclerostin. (d) Wnt-reporter assays show that sclerostin from Sf9- or bacterially expression system is active as seen from the dose-dependent inhibition of Wnt-activity. (e) Full-length and C-terminally truncated sclerostin exhibit identical activity, whereas N- and C-terminally truncated sclerostin shows a 3-5fold lower Wnt inhibition.*

As crystallization failed,NMR-spectroscopy was used for structure determination of free sclerostin using the sclerostin variant SOST_ΔNC (Fig. 4.4). The structure of sclerostin shows no similarity with other known protein structures [E1]. The two loops (loop 1 and 3) emanating from the cystin-knot into the same direction form two short two-stranded β-sheets resembling two fingers (Fig. 2). The two fingers cross each other at the tips of the fingers with the orientation of the two fingers being stabilized by a disulfide bond between the two fingertips. The loop 2 displays no regular secondary structure and superposition of the NMR structure ensemble suggests that this loop is highly flexible [E1] (Fig. 2). NMR relaxation analysis is currently performed; preliminary results indeed show that loop 2 is highly dynamic and disordered in the absence of a binding partner (Weidauer, S & Mueller, T., unpublished). In an independent study M. Carr and colleagues determined the structure of full-length human sclerostin [16] confirming our results and showing that the termini are indeed flexible.

As expression of LRP5 failed, only very small amounts of the extracellular domain or the E1E2 truncated domain of hLRP5 could be obtained from HEK293T cells, structural and

functional studies involving LRP5 protein were not possible. However, a 3D homology model on the basis of the LDLR receptor covering the first two YWTD propeller domains was generated. Docking studies were performed using the structure of the complex of laminin and nidogen, but the structural similarity between laminin and sclerostin is very limited, so placement of sclerostin on the top of the first propeller is very preliminary.

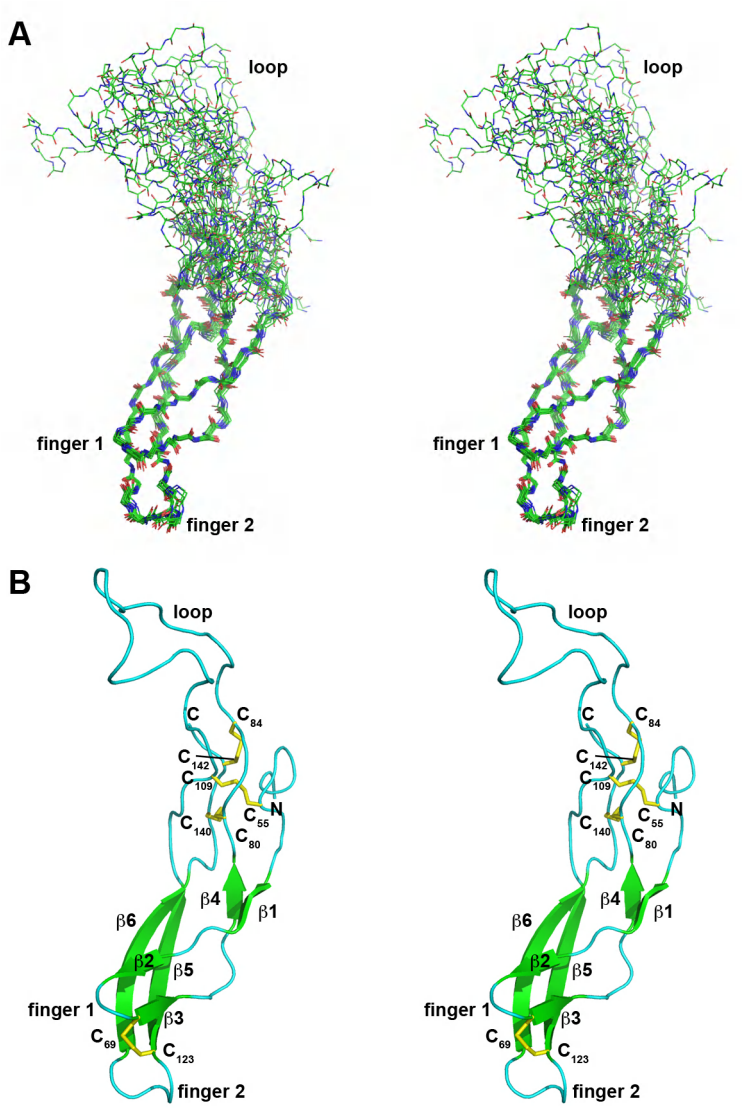

Figure 4.4: *(a) Stereoview of a structural ensemble of 15 structures of murine sclerostin SOST_ΔNC aligned to the structured regions termed finger 1 and 2, only backbone atoms are shown. The loop is disordered. (b) Secondary structure sketch of murine sclerostin SOST_ΔNC, β-strands are indicated as green arrows and numbered according to their appearance, disulfide bonds are indicated as yellow sticks.*

Thus, analysis of the electrostatic potential was used to check for complementary properties in the propeller 1 of LRP5, which is the likely binding site for sclerostin and LRP5. This analysis indeed showed the first β-propeller of LRP5 and sclerostin exhibiting an unusual highly complementary charge distribution suggesting that either the finger 1 or the loop of sclerostin might harbor the binding site of sclerostin to LRP5 [E1].

Beneficiary 5 has recently made progress in obtaining an expression system for LRP6 sufficient to produce protein quantities for functional studies. Two approaches were used, expression of LRP6 E1E2 and E1 alone in baculovirus transfected insect cells. Whereas regular Sf9 or Sf21 cells were found to produce only very minor amounts of LRP6, application of a new established system of *Trichopulsia ni* cells growing in suspension cultures of serum-free medium allowed to obtain 10fold larger yields. In addition, expression is currently tested in suspension-culture 293 FreeStyle (Invitrogen) cells that are transiently transfected. Similar to the insect cell expression system, these cell line provide larger yield of secreted LRP6 protein, when the secretion chaperone MesD is coexpressed. Beneficiary 5 is currently trying to produce recombinant LRP6 from these two sources for structural and functional analyses and has thus applied for national funding for follow-up studies.

Functional description of the binding epitopes and main binding determinants of sclerostin and LRP5.

To obtain a description of the functional epitope of sclerostin we first analyzed the hypothesis that the charge complimentary (highly basic) regions of sclerostin are involved in the interaction with LRP5/6. Thus an alanine scanning mutagenesis was performed, exchanging all arginine residues within the cystin-knot region and determining the Wnt-inhibition activity of these sclerostin variants in an established Wnt-reporter assay. The assay initially established was based on HEK293T cells that were transiently transfected with the Super TopFlash reporter plasmid obtained from Randall Moon's lab. However, the quality of the transiently transfected reporter cells proved to be to varying for a more quantitative analysis, and thus UWUE established the generation of a stably transfected reporter cell line for the functional studies (Weidauer, S. & Mueller, T. unpublished). Employing this assay we could obtain quantitative IC50 values for all sclerostin variants obtained in our mutagenesis study. Of the 14 arginine residues present in the sclerostin truncation variant SOST_ΔNC 11 arginine-to-alanine single amino acid variants were prepared and tested in the Wnt-reporter assay. However no complete abrogation of Wnt-inhibition could be determined for any of these variants. This observation and the data published by the group of M. Carr showing that a neutralizing antibody bound to the loop region of sclerostin suggested that either the arginine residues play no major role for maintaining sclerostin activity/binding or binding to LRP5 is not the activity-determining step for sclerostin. Analysis of a Fab against murine sclerostin developed with beneficiary 10 confirmed this finding. The Fab AbD09097 neutralizes sclerostin activity in the Wnt reporter assay in a dose-dependent manner, mapping of the Fab's binding site on sclerostin using NMR chemical shift mapping (*Manuscript in preparation*) showed that the majority of the Fab AbD09097 binding site is located at the tip of the loop in sclerostin.

Due to the new data suggesting that the loop region is involved in mediating sclerostin-dependent Wnt-inhibition we have revised the mutagenesis study and prepared additional sclerostin variants with single amino acid exchanges covering the loop region. Together with variants in which the loop region was either truncated or exchanged against a scrambled sequence as well as two mutants in which the surface oriented amino acids in either finger 1 or finger 2 were exchanged against a scrambled amino acid sequence a detailed analysis of the regions involved either in binding to LRPs or covering parts important for sclerostin's activity could be performed. Analysis using the Wnt-reporter assay showed that most of the sclerostin variants retained their Wnt-inihibitory activity, but truncation of the loop region (Leu90 to Asn103) or exchange of these residues with a random Gly/Ser/Ala sequence completely

decreased the activity (Fig. 4.5, *Manuscript in preparation*). Single amino-acid exchanges in this loop showed only minor effects suggesting that either side chain do not mediate the activity or that loss of only one side chain does not affect activity.

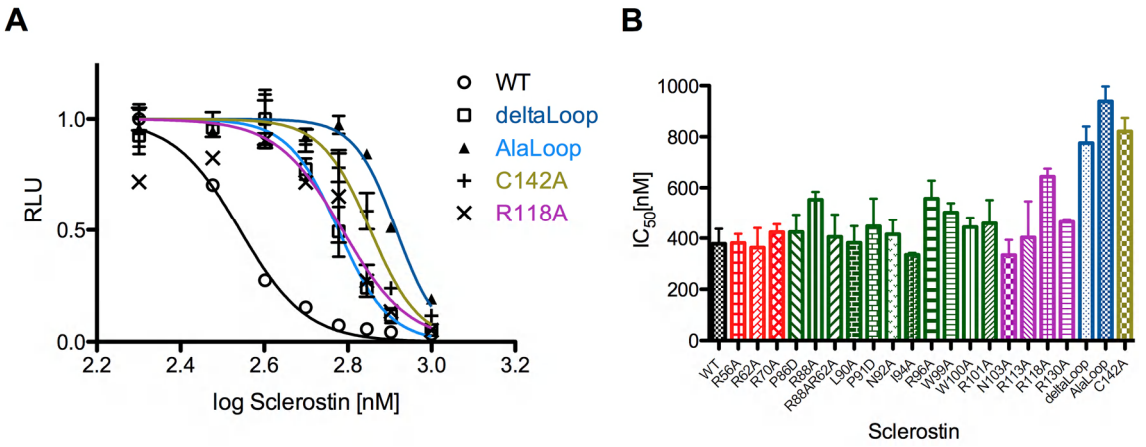

Figure 4.5: *Analysis of single amino acid and multi-mutant sclerostin variants using the Wnt-reporter assay in HEK293T cells stably transfected with the SuperTop Flash reporter. Variants with truncation in the loop region of sclerostin or a scrambled loop region show an attenuated sclerostin activity (2-fold). Additionally, mutations in finger 2 or the cystin-knot region also affect sclerostin-mediated Wnt-inhibition.*

Besides altering the loop region, which confirmed the data obtained from the neutralizing antibody Fab AbD 09097, also the "multi-"mutant, in which all surface-located amino acid residues in finger 2 were exchanged to either Gly, Ala or Ser residues, showed an attenuated inhibition of Wnt activity in the reporter assay. Furthermore, three mutants with mutations in either finger 2 or the cystin-knot region (R118A, C142A, and R118A/R144A) also exhibited an decreased Wnt-inhibitory activity (Fig. 4.5).

These findings suggest that two regions in sclerostin are required for Wnt-inhibition activity, the loop region covering the loop tip as well as the finger 2/cystin knot region. To test whether both epitopes are involved in binding to LRPs we have in collaboration with beneficiary 1b performed binding studies using chemical crosslinking of radiolabled sclerostin to COS7 cells transiently expressing LRP6. Surprisingly this experiment shows that the loop region is responsible for binding of sclerostin to LRP6, whereas mutations in finger 2 (as well as the single and double amino acid mutations mentioned above) do not affect binding of sclerostin to LRP6 despite its diminishing effect on sclerostin-mediated Wnt-inhibition (Fig.4.6) (*Manuscript in preparation*).

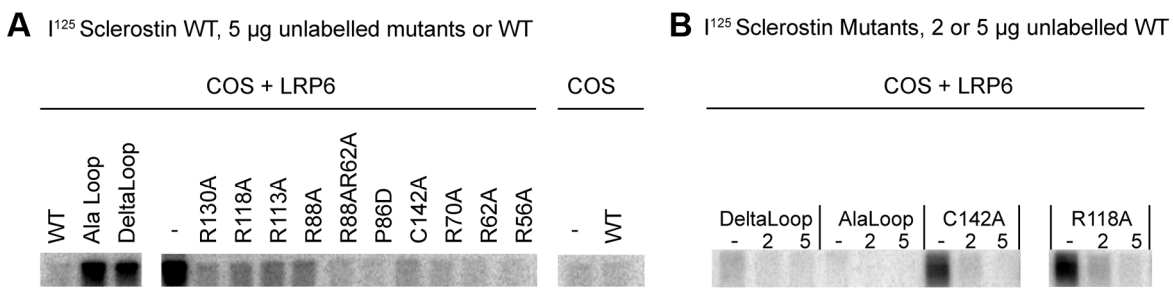

Figure 4.6: *Binding analysis of sclerostin to LRP6 on transfected cells. Radioactively I^{125}-labeled wildtype sclerostin was chemically crosslinked in the presence of sclerostin variants and analyzed by autoradiography. Mutants still capable to bind to LRP6 compete with the radiolabeled sclerostin for binding and thus displace the radiolabeled sclerostin, whereas M mutants impaired in binding to LRP6 cannot displace the probe (e.g. see panel A Ala Loop and Delta Loop). The experiment was repeated with the variants labeled and competition using unlabeled wildtype sclerostin (panel B).*

Of particular interest is the sclerostin variant C142A, for which a similar mutation C142R has been discovered as the first missense mutation in patients suffering from sclerosteosis. Although a possible effect on the folding of the loop region cannot be excluded from modeling [E2], in the light of these new results it seems that Cys142 and a part of the cystin knot also form a new binding epitope to a possibly second, yet unknown binding partner/receptor for sclerostin. As these variants with an impaired epitope 2 can still bind to LRP6 but show a strongly reduced bioactivity these variants might possibly represent sclerostin antagonists. We are currently performing experiments in collaboration with partner 6 Serge Ferrari, University Geneva to test this hypothesis. All recombinant proteins were also made available to all consortium partners (Beneficiaries 1b, 8 and 10).

Antibody against peptides derived from sclerostin that interact with BMP or LRP5 and from LRP5 that interact with sclerostin

The task of beneficiary 10 was to generate antibodies directed against sclerostin. Two main approaches were performed, either peptides provided by beneficiary 8 and mimicking different parts or full-length sclerostin (Fig. 4.7) were used to select antibodies from a library using phage display, or alternatively, recombinant proteins were employed in this selection procedure. All antibody fragments were generated using the HuCAL phage antibody libraries and using antigens either biotinylated or in the case of peptides coupled to BSA in a so-called solution panning.

Figure 4.7: *Sequences of recombinant human and murine sclerostin, made by beneficiary 5 (UWUE), aligned with the mimics generated by beneficiary 8, the boxed green areas indicate the epitope cores of the Fabs provided by beneficiary 10*

Biotinylated antigens were incubated with the HuCAL library and binding phage were rescued using streptavidin coated magnetic beads. After three rounds of panning the enriched pool of Fab genes was isolated and inserted into an E. coli expression vector that leads to functional periplasmic expression of monovalent Fab which are equipped with two peptide tags, the myc-tag and a His_6-tag at the C-terminus of the F_H chain, which can be used for antibody purification and detection. All Fabs also contain a thrombin cleavage site, which can be used to cleave off the tags in case the additional amino acids interfere with crystal formation for the structural studies. For each panning, 368 clones were tested in an ELISA screening for specific binding to the selected antigens. For the peptides provided by beneficiary 8 (PEPSCAN) antibodies were generated by beneficiary 10, of which many also bind sclerostin as tested in SPR experiments performed by beneficiary 5; in total, 42 different Fabs could be obtained for the peptides mimicking finger 1 and 2 of which 15 bind also to sclerostin with high affinities in the nano-molar range. Twentyone Fabs (from different conformers) could be obtained for the peptide mimicking the loop of sclerostin, which has been identified to be required for sclerostin Wnt-inhibitory activity. Five out of these 21 Fabs bound the loop of sclerostin with high affinity and are tested with respect to sclerostin-neutralizing activity. One of them (AbD 10764) indeed neutralized sclerostin activity in a Luciferase assay performed by beneficiary 5.

An interesting finding was that none of the Fabs from the panning on the constrained SYM117 binds the linear SYM117 peptide, while all Fabs from the panning on linear SYM117 also bind the constrained peptide (Fig. 4.8). Furthermore, the antibodies from the panning on constrained SYM117 show on average a much better binding to human and murine sclerostin in ELISA, indicating that the constrained structure resembles the folded protein.

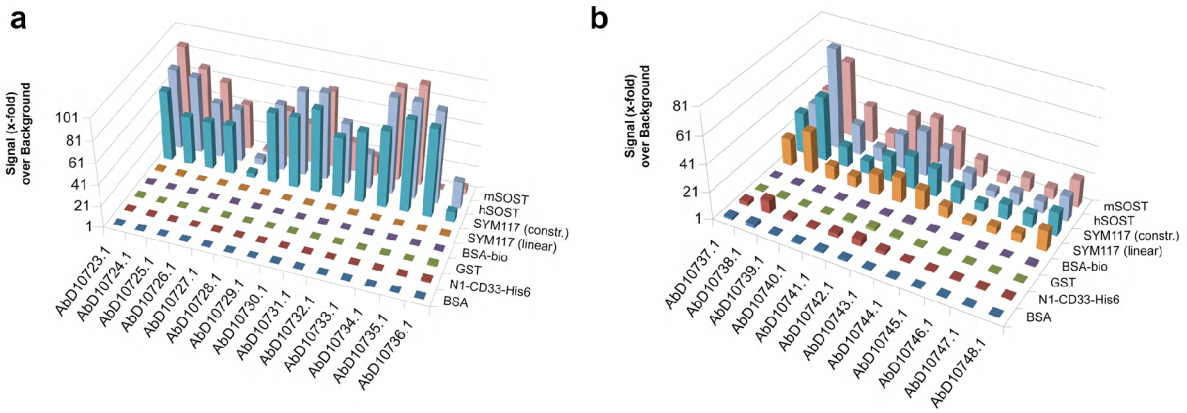

Figure 4.8: *ELISA testing of antibodies from panning on constrained and linear SYM117 peptide. Various control proteins BSA, CD33 and GST confirm the antigen-specificity of the selected antibodies.*

Antibodies and peptides have been also sent to beneficiary 5, where the Fabs have been characterized by SPR methodology and are currently tested for neutralizing activity in the Wnt reporter assay. As most of the antibodies derived by the different antigen selection procedures yielded Fab antibodies directed against the core-part, similar to the core protein SOST_ΔNC another approach was applied by beneficiaries 8 and 10 to selectively obtain antibodies directed against either the N- or C-terminus of sclerostin. Peptides encoding for both termini (SYM 594, SYM595 and SYM596) were used for the panning, SYM594 and SYM595 were coupled to BSA, which was then immobilized on magnetic beads using thiol-chemistry, and the biotinylated peptide SYM596 was used via streptavidin magnetic beads.

Three Fabs could be selected against the peptide mimicking the C-terminus of sclerostin, however, only one Fab AbD13031 bound sclerostin with rather low affinity. In contrast, 12 Fabs could be selected against the N-terminus of sclerostin, of which 7 bind also to sclerostin. The antibodies have been epitope mapped by beneficiary 8, to ensure that the antibodies recognized the intended area. One antibody was found to cross-react with a pseudo-repeat in the cystin knot region, making it not specific for the C terminus. Two Fabs seem species-specific and bind only to human sclerostin (AbD13099 and AbD13100), the best Fab recognizing the N-terminus of sclerostin exhibits an affinity in the low nanomolar range and binds to human and murine sclerostin (AbD13102). The latter Fab might be a useful tool for the analysis and detection of sclerostin degradation in vivo since in vitro experiments of sclerostin derived from eucaryotic cell culture showed rapid proteolytic degradation of the flexible termini.

In addition to the peptides, also human and murine sclerostin proteins prepared by beneficiary 5 have been provided to beneficiary 10 (ABD) for the production of antibody Fab fragments. The antibody fragments were generated using the HuCAL phage antibody libraries and recombinant biotinylated human and murine sclerostin in a so-called solution panning similar to the procedure described for the peptides.

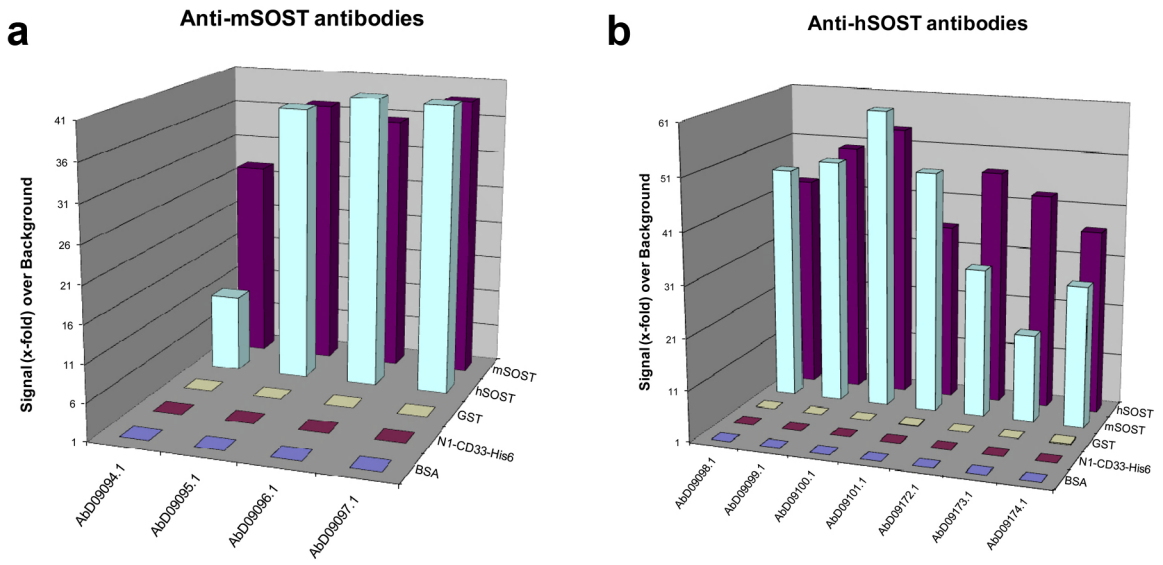

Figure 4.9: *ELISA testing of antibodies from panning on murine (a) and human (b) recombinant sclerostin.*

From the panning using murine sclerostin four unique Fabs (designated AbD09094, AbD09095, AbD09096 and AbD09097) and from the panning using human sclerostin seven unique Fabs (designated AbD09098, AbD09099, AbD09100, AbD09101, AbD09172, AbD09173 and AbD09174) were obtained. These 11 recombinant antibody Fab fragments were expressed on a larger scale, purified and tested again in ELISA on murine and human sclerostin and on unrelated control proteins (Fig. 4.9). Specific binding to sclerostin could be confirmed for all antibodies. One Fab from the panning on murine sclerostin (AbD09094) showed a better binding on the murine antigen and three Fabs from the panning on human sclerostin (AbD09172, AbD09173 and AbD09174) a better binding on the human antigen. The purified Fabs were sent to beneficiaries 5 and 8 for further characterization. The antibodies were tested for sclerostin binding using surface plasmon resonance (SPR) to obtain quantitative information for binding affinity and specificity, which confirmed most of the above characterization. Despite the fact that full-length sclerostin proteins were used for selection of the Fab antibody fragments all non species-specific Fabs obtained bind the N- and C-terminally truncated murine sclerostin (SOST_ΔNC) with very similar affinity compared to full-length protein (reference: murine sclerostin) with a difference in affinity of less than 2-fold. This indicates that the binding epitopes for all antibody fragments reside inside the structured core of sclerostin. One antibody (AbD09094) is highly specific for murine sclerostin, while AbD09173 binds with high specificity to human sclerostin exhibiting a 240-fold lower affinity for the murine sclerostin variant SOST_ΔNC. Almost all antibodies bind sclerostin with low nano- to subnanomolar affinities and thus exhibit a very high binding affinity for the antigen already without additional affinity maturation (*Manuscript in preparation*). In addition to SPR interaction analysis of the antibodies we started to test their ability to neutralize sclerostin-mediated Wnt-inhibition using the Wnt reporter assay. Four of the originally derived Fabs have been analyzed via this assay, revealing that Fabs AbD09094, AbD09100 and AbD09101 bind sclerostin without altering its Wnt-inhibition activity, whereas Fab AbD09097 is able to neutralize sclerostin-mediated Wnt-inhibition with very high efficiency (Fig. 4.10).

To obtain information about the binding epitope(s) of the Fab antibodies beneficiary 8 performed mapping analyses using their unique peptide epitope mapping technique. Since the lack of a source for recombinant LRP5, it was not possible to probe the binding of LRP5 on sclerostin derived peptide arrays, these arrays have thus been put to use in profiling the epitopes of the antibodies generated by beneficiary 10. For eight of the 11 Fab fragments potential binding sites could be derived from the mapping study suggesting that the non-neutralizing Fabs AbD09094, 09100 and 09101 bind either at the N-terminus or finger 2 of sclerostin, whereas sclerostin-neutralizing AbD09097 is the only Fab that binds in the unstructured loop).

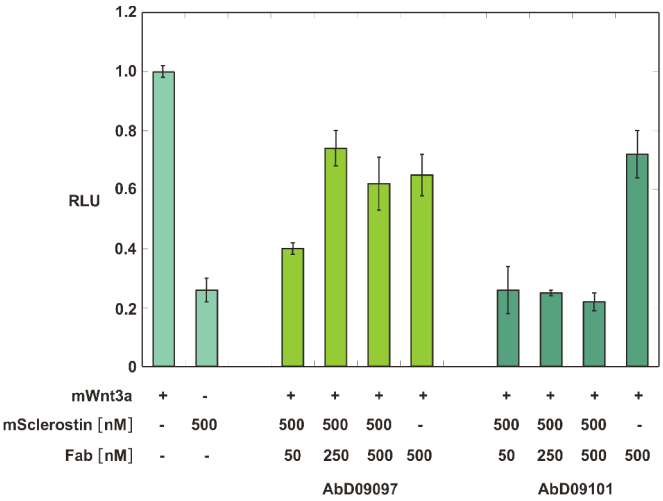

Figure 4.10: *Wnt-reporter assay showing that the Fab antibody fragment AbD09097 efficiently relieves Wnt-activity from sclerostin inhibition. Due to the high affinity of AbD09097 for murine sclerostin, a 0.1 molar equivalent of AbD09097 is sufficient to block sclerostin. The non-neutralizing AbD09101 shows no sclerostin-inhibition, thus sclerostin does neutralize Wnt-activity also in the presence of this antibody.*

The binding of neutralizing Fab AbD09097 was fine mapped with a custom designed library, containing hundreds of variants of the best binding peptides, thus allowing to determine the binding site of the Fab at sclerostin. A mapping was also performed using the 20 sclerostin variants (see deliverable 4.3) and SPR. Here, sclerostin variants were immobilized on the biosensor and the affinities of all Fab proteins were determined to wildtype and variant sclerostin using the unique one-shot kinetics and high-throughput capabilities of the Biorad ProteOn X36 SPR system. Thereby an interaction map could be generated allowing to define the binding sites of these Fabs directly on sclerostin. These data were then compared with the results of the peptide mapping study.

In addition, an NMR-mapping study, in which uniformly ^{15}N-labeled sclerostin was titrated with different Fab proteins and the change of the amide nitrogen-proton signal was monitored in 2D ^{1}H-^{15}N correlation spectra. From this analysis the binding site of Fab AbD09097 could be unambiguously defined to the loop tip of the unstructured loop of sclerostin. NMR mapping studies were also performed for the several non-neutralizing Fabs, preliminary data confirm that the Fabs AbD09094, AbD09100 and AbD09101 bind to the finger regions or the N-terminus (*Manuscript in preparation*). On the basis of the biochemical and cell-based data Fab AbD09097 presents a highly valuable tool due to its neutralizing ability and can be used to study the receptor of sclerostin and its Wnt-inhibition mechanism.

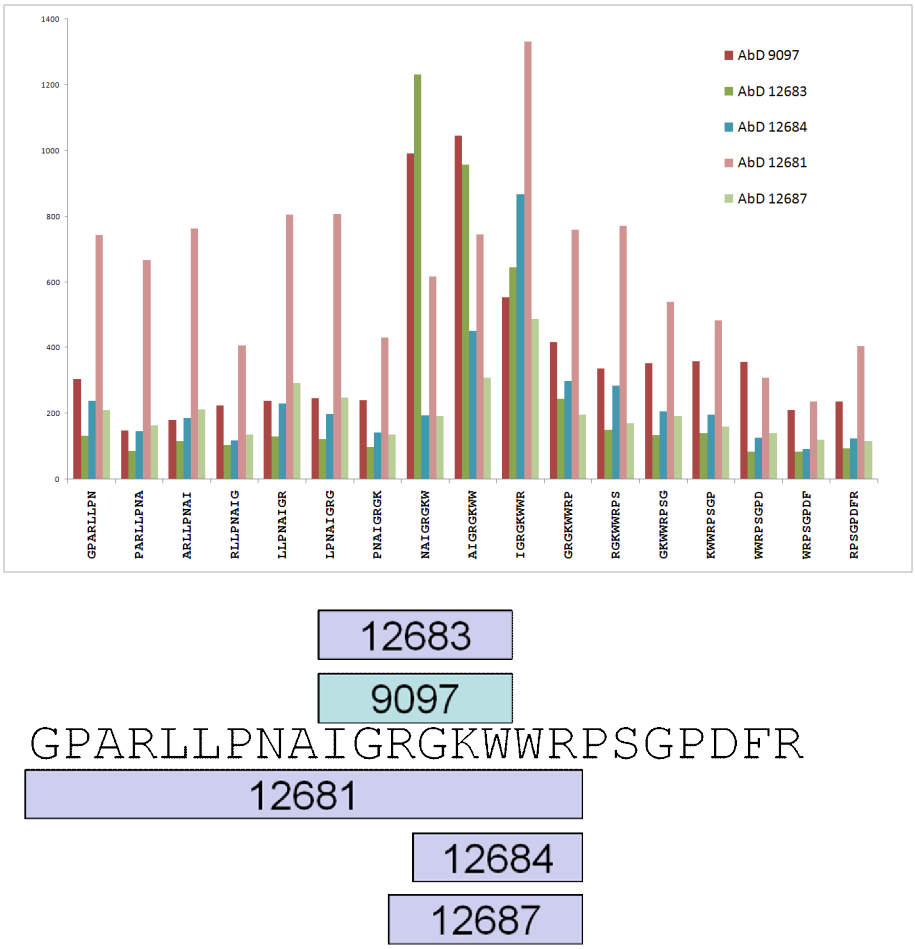

Figure 4.11: *High resolution mapping using pepscan arrays of Fab AbD9097 and affinity matured derivates on a library consisting of all 4 mer, 5mer, 6 mer peptides up to full length 24 mer of the sclerostin finger 24 region. Upper panel) Binding to all overlapping 8 mers. Lower panel) Epitope cores of the different Fabs that have been mapped.*

Therefore beneficiary 10 performed an affinity maturation process using AbD09097 as a start template. To do so, CDR 3 of the light chain was replaced by a highly diverse CDR3 cassette thereby generating a library of $3x10^6$ different clones. This library was then subjected to solution panning as described above with decreasing amounts of biotinylated sclerostin for the capture step and more stringent washing. From 100 hits the 20 clones giving the highest signal in the ELISA were sequenced. From these seven unique new antibodies (AbD12681-AbD12687) were obtained and analyzed by SPR by beneficiary 5. Of these seven "matured" antibodies all show at least two-fold improved affinity to murine sclerostin and at least seven-fold increased affinity to human sclerostin. Very good "binders", e.g. AbD12682, AbD12683 and AbD12686, bind murine sclerostin with the subnanomolar affinities and to human sclerostin with very low nanomolar affinity. To obtain data on the possible differences in the binding epitope of these matured antibodies on sclerostin beneficiary 8 has mapped the AbD9097 and its derivates AbD12681-12687 on a high resolution pepscan library, comprising all overlapping 4 mer, 5 mer, 6 mer peptides up to the full 24 mer peptide spanning the finger 2 region (Fig. 4.11).

To enhance sensitivity of the neutralizing antibody AbD09097 in assays like immunohistochemistry or Western Blotting the Fab gene was also subcloned into different formats. A bivalent antibody with the format Fab-dHLX-MSx2 was obtained, which contains a heavy chain C-terminal dHLX-dimerization domain followed by a Myc and a double extended Strep-tag. Due to its bivalent nature the affinity of the original AbD09097 is enhanced to sclerostin due to avidity effects. Additionally, two full-length IgG formats, a human/mouse IgG1 (human VL and VH, mouse constant domains) and a human/mouse IgG2a (human VL and VH, mouse constant domains) were obtained, which allow for in vivo analysis in immunohistochemistry in either mouse or human tissues.

Since the mapping and mutagenesis studies revealed the loop region of sclerostin to be the determinant for sclerostin's activity we have also setup a guided selection procedure to directly obtain a sclerostin-neutralizing Fab. Recombinant human and murine full-length sclerostin was biotinylated and coupled to magnetic streptavidin beads.

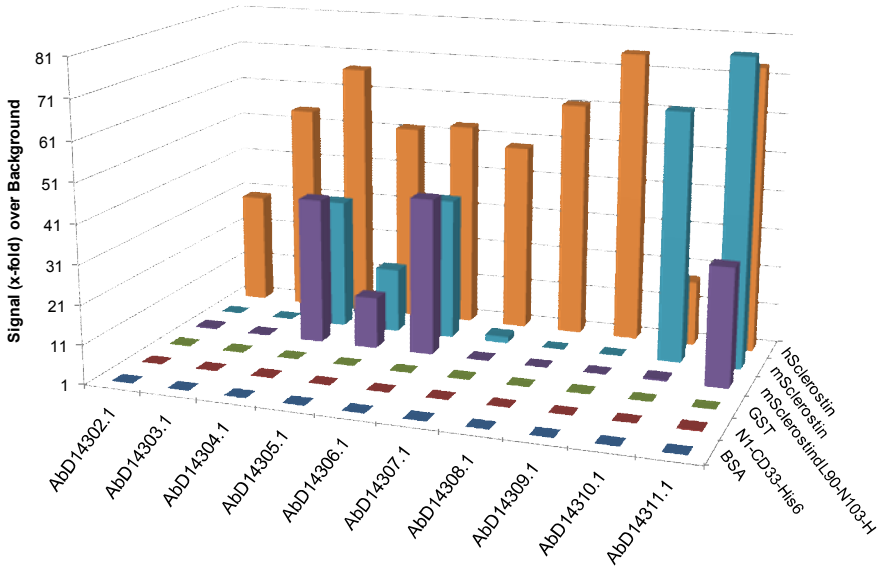

Figure 4.12: *ELISA testing of antibodies from panning on human (AbD14302-9) and human (AbD14310-1) recombinant sclerostin. To obtain specifically sclerostin-neutralizing Fabs, a sclerostin truncation variant lacking the loopregion was used for blocking during the phage-display panning procedure.*

During solution panning the binding of Fab-expressing phage was blocked by a sclerostin truncation variant lacking the loop region, i.e. Leu90 to Asn103, thus increasing the fraction of retained phages, which carry Fabs binding to this region of sclerostin. From the guided-selection 10 new different Fabs could be identified in ELISA analysis by beneficiary 10 (Fig. 4.12). All 10 Fabs were analyzed by SPR by beneficiary 5 for their binding to human and murine sclerostin and their binding epitope was mapped using single amino acid and truncation sclerostin mutants. Of the 10 new Fabs the antibody AbD14310 had the best properties and was tested in the Wnt-reporter assay for its neutralizing activity showing that it can indeed efficiently and dose-dependently restore Wnt-activity from sclerostin inhibition. A comparison of both neutralizing antibodies AbD09097 and AbD14310 shows that both Fabs exhibit different binding properties for sclerostin and also seem to recognize overlapping but

slightly different epitopes (*Manuscript in preparation*). As both neutralizing antibodies provide very valuable tools large scale preparations were performed by beneficiary 10 and the proteins were provided to beneficiary 5 for structural and functional analyses.

Molecular description of sclerostin-LRP5, sclerostin-Fab, and LRP5-Fab complexes

To understand the molecular mechanism of sclerostin binding to the Wnt coreceptors LRP5/6, structural analysis of the complex of sclerostin bound to the extracellular domain of LRP5 or LRP6 via X-ray crystallography was proposed. However, due to severe difficulties in the expression and production of recombinant LRP proteins (see also deliverable 4.3) these tasks as well as the structure analysis of LRP5-Fab complexes could not be achieved within the timeframe of the EU project TALOS. Very recently beneficiary 5 made progress in obtaining an expression system in baculovirus-transfected insect cells (a new high-expressing strain of insect cells adapted to serum-free suspension culture conditions was used), which provides with recombinant LRP6 (full length extracellular domain) in the 100 to 200 µg per Liter culture scale. In addition, beneficiary also tries to express the ectodomain of human LRP6 in suspension culture adapted 293 cells (FreeStyle 293T cells, Invitrogen), which proved to be very efficient in the expression of LRP6. First results are promising and the quantities of recombinant LRP6 obtained by these two approaches seem to be sufficient to at least allow for functional in vitro interaction analysis studies. Besides functional studies, beneficiary 5 also tries to optimize expression yields for structure determination in future studies.

To obtain insights into neutralization mechanism of the two sclerostin-neutralizing antibodies AbD09097 and AbD14310, beneficiary 5 has started crystallization trials involving both Fabs. Initial experiments focus on the crystallization of the Fab proteins alone, first crystal for the sclerostin-neutralizing Fab AbD09097 have been already obtained. Crystallization is currently optimized to yield large single crystals suitable for structure determination by X-ray diffraction .After obtaining first data sets for the anti-sclerostin Fab proteins, protein complexes of sclerostin bound to either one of the neutralizing Fabs will be subjected to crystallization trials.

Workpackage 5: Intervention strategies that target sclerostin function.

Objectives:

- In vitro and in vivo characterization of peptide-based protein mimics to affect LRP5-mediated canonical Wnt signaling and bone formation.

In vitro characterization

Using our proprietary algorithm, we have identified a number of characteristics within the sclerostin molecule, including putative cleavage sites. Two of the identified cleavage sites are ADAM7 and a convertase (*e.g.* proconvertase or furin). In being cleaved once or twice, different *SOST* fragments may be being generated which could give different functionalities. The third cleavage site identified from the algorithm is caspase 9, which activates the

apoptotic pathway. The N-terminus fragment of sclerostin was identified to have homology with p53-binding protein (53BP2) which is involved in apoptosis. This may account for why *SOST,* when overexpressed in some cell lines, kill the cells prematurely. Currently, fragment specific antibodies against the central *SOST*, C-terminus and N-terminus fragments are being synthesised by beneficiary 10, to assist us in validating the computational finding. Experiments have been designed to test the effect of these antibodies on Wnt-signaling in KS483 cells. However, results are not available yet.

Characterization of peptide-bound protein (sclerostin) mimics to modulate bone formation in vivo

The aim of this project was to test whether SYM1318ox, a peptide mimetic designed as a potential antagonist of sclerostin, would increase bone mass and structure in growing mice. As a positive control, we used mechanical loading of the tibia, which was previously demonstrated to suppress sclerostin expression and induce an anabolic bone response in the loaded bone specifically. The peptide SYM1318ox, designed and synthetized by Pepscan Therapeutics, is the homolog of the oxidized b2 loop of the sclerostin. To test this analogue of sclerostin, 3 month-old female C57Bl/6 mice were treated subcutaneously for 14 days with SYM1318ox (0.01 and 0.1 mg/day) or vehicle by osmotic mimipumps (Alzet®). Simultaneously, the left tibia of each mouse was subjected to an axial compression (12N, 2 Hz) 7 min every other day. The right tibia was used as the unstimulated control. There were 6-7 mice/group. Bone mass and body composition changes were assessed longitudinally by densitometer (DXA). After 14 days of treatment, mice were sacrificed and bones were collected for evaluation of the microarchitecture, blood was sampled for measurements of bone turnover markers (osteocalcin and CTX).

Results are presented below in 2 tables. Overall, SYM1318ox did not improve bone mass (BMD, BMC) in the whole skeleton nor spine, although at the lowest dose it had a small but significant effect on BMD in the unstimulated tibia. This effect however was much less than the effects of mechanical loading (loaded tibia) on BMD, and there was not additive/synergistic effects between SYM1318ox and mechanical loading. SYM1318ox also did not improve cancellous nor cortical bone architecture in the unloaded nor loaded tibia. Actually, at the highest dose (0.1 mg/d), it tended to *decrease* tibia BMD and BMC, cancellous BV/TV and connectivity density, as well as cortical bone volume compared to the lowest dose (0.01 mg) and vehicle, suggesting that at this dose, SYM1318ox might have some sclerostin-like agonistic activity. Alternatively, at the highest dose SYM1318ox could have some toxic effects, as suggested by a decrease in body weight and percentage fat in the treated animals. To note that biochemical markers of bone resorption (CTX) was increased at the highest SYM1318ox dose, whereas a marker of bone formation (osteocalcin) was unaffected.

Table 5.1. Effects of the sclerostin peptide mimetic SYM1318ox on body composition and bone in mice

	Vehicle	SYM1318ox 0.01 mg	SYM1318ox 0.1 mg	P treatment
Body Composition Change over 14 days				
Body weight gain (g)	1.52±0.43	1.34±0.25	0.62±0.11*	0.079
% fat change (14-0)	2.58±0.52	1.57±0.39	0.70±0.65*	0.075
Lean change (g) (14-0)	0.40±0.26	0.17±0.15	0.13±0.17	NS
Bone Mass Change				
Total Body BMD change (mg/cm^2)	-0.017±0.30	0.043±0.39	-1.0±0.43	NS
Total Body BMC change (mg)	6.5±3.4	9.04±3.7	-5.0±5.6	0.078
Spine BMD change (mg/cm^2)	-1.9±2.1	-3.9±1.9	-2.3±2.1	NS
Spine BMC change (mg)	0.12±0.85	-0.87±0.35	-1.07±0.6	NS
Vertebral microarchitecture at 14 days				
BV/TV (%)	17.36±0.88	17.83±0.73	15.53±0.63#	0.09
Tb Number (/mm)	4.37±0.11	4.35±0.10	4.04±0.16	NS
Markers of bone turnover				
CTX change (ng/mL)	5.9±1.5	4.6±0.9	16.8±3.2*#	0.0016
Osteocalcin at 14 days (ng/mL)	149.5±9.2	121.0±7.8	122.1±6.0	0.0322

*, $P<0.05$ compared to veh

Table 5.2. Effects of the sclerostin peptide mimetic SYM1318ox in combination with mechanical loading on mouse tibia

	Vehicle		SYM1318ox 0.01 mg		SYM1318ox 0.1 mg		P treatment	P stimulation	P interaction
	UN	STI	UN	STI	UN	STI			
Tibia BMD (mg/cm^2)	51±1	61±1	53±1*	61±1	50±1#	60±1	NS	<0.0001	NS
Tibia BMC (mg)	66±2	62±1	67±1	64±1	64±1#	60±1	0.0166	NS	NS
Tibial Cortical Microarchitecture									
TV (mm^3)	0.697±0.018	0.705±0.016	0.718±0.023	0.723±0.025	0.653±0.006#	0.687±0.006	0.0122	NS	NS
BV (mm^3)	0.412±0.016	0.417±0.008	0.419±0.012	0.444±0.017	0.379±0.005#	0.417±0.006	0.0153	0.0194	NS
Cort thickness (□m)	208.8±7.6	217.8±4.3	208.7±5.3	226.5±5.3	202.7±2.5	218.7±2.3	NS	0.0006	NS
Tibial Cancellous Microarchitecture									
BV/TV (%)	3.35+0.28	7.08±0.33	3.58±0.34	6.42±0.80	2.65±0.16#	4.91±0.38	0.0086	<0.0001	NS
Tb Th (□m)	44.45±1.33	58.66±2.02	44.66±1.47	55.43±2.88	42.61±1.73	51.60±1.52	NS	<0.0001	NS

Tb N (/mm)	2.37±0.17	2.68±0.13	2.52±0.07	2.67±0.09	2.47±0.11	2.31±0.20	NS	NS	NS
Connectivity density	7.7±2.3	22.1±2.51	9.2±1.2	17.3±3.3	4.5±0.9#	13.3±1.4	0.203	<0.0001	NS

UN=unstimulated, STI= stimulated ; *, p<0.05 vs Veh ; #p<0.0 vs SYM1318ox 0.01mg

We next tested a second mouse sclerostin peptide mimetic, R118AR1441A, designed and synthetized by beneficiary 5.

The doses tested were 0.01 and 0.05 mg/d. Results are presented in tables below. R118AR1441A at the doses tested did not modify weight nor body composition, but significantly increased total body BMD and BMC gain. However the compound had no effects on cancellous and cortical microarchitectures of the unloaded tibia. The co-treatment (R118AR1441A and mechanical stimulation) did not induce an additive effect, except for a trend of increased cortical thickness at the midshaft tibia. Bone turnover markers did not significantly change upon treatment, although there was a trend for the highest R118AR1441A dose to sustain osteocalcin levels.

Table 5.3. Effects of the sclerostin peptide mimetic R118AR1441 on body composition and bone in mice

	Vehicle	R118 0.01 mg	R118 0.05 mg	P treatment
Body Composition Change over 14 days				
Body weight gain (g)	1.34±0.43	1.67±0.17	1.64±0.16	NS
% fat change (14-0)	-1.1±0.87	-1.4±0.6	-0.5±0.4	NS
Lean change (g) (14-0)	1.2±0.1	0.8±0.2	1.0±0.2	NS
Bone Mass Change				
Total Body BMD change (mg/cm^2)	-0.10±0.29	1.23±0.46*	1.27±0.26*	0.261
Total Body BMC change (mg)	13.12±6.61	31.40±6.60*	21.83±3.66	NS
Spine BMD change (mg/cm^2)	-0.67±2.17	0.59±1.63	1.71±2.0	NS
Spine BMC change (mg)	0.27+0.62	0.31±0.46	1.61±0.62	NS
Vertebral microarchitecture at 14 days				
BV/TV (%)	18.47±0.97	18.33±1.47	18.22±0.93	NS
Tb Number (/mm)	4.54±0.15	4.47±0.22	4.29±0.17	NS
Tb Thickness (□m)	44.4+0.6	44.9+1.1	46.2+0.8	ns
Markers of bone turnover				
CTX change (ng/mL)	-5.8±1.7	-2.7±1.9	-5.6±2.0	NS

Osteocalcin change (ng/mL)	-18.5±23.2	-17.01±21.4	10.0±31.4	NS

*p0.05 vs Veh

In conclusions, neither of the sclerostin peptide mimics tested showed clear anabolic effects on the skeleton, particularly not in the tibia and as compared to mechanical loading. Hence these particular compounds are unlikely to function as efficient sclerostin antagonists in vivo.

Table 5.4. Effects of the sclerostin peptide mimetic R118AR1441 in combination with mechanical loading on mouse tibia

	Vehicle		R118 0.01 mg		R118 0.05 mg		P treatment	P stimulation	P interaction
	UN	STI	UN	STI	UN	STI			
Tibia BMD (mg/cm^2)	42.9±1.0	47.8+1.1	41.8±0.5	48.6±1.0	42.5±0.6	48.5±0.6	NS	<0.0001	NS
Tibia BMC (mg)	14.5±0.4	13.6±0.5	14.0±0.3	13.4±0.3	14.2±0.4	13.3±0.4	NS	0.0128	NS
Tibial Cortical Microarchitecture									
TV (mm^3)	0.673±0.019	0.690±0.09	0.665±0.014	0.694±0.011	0.669±0.012	0.699±0.07	NS	0.018	NS
BV (mm^3)	0.374±0.009	0.396±0.001	0.374±0.005	0.399±0.007	0.382±0.007	0.408±0.005	NS	<0.0001	NS
Cort thickness (□m)	195.5±3.0	204.8±2.8	196.0±2.4	205.0±3.6	199.3±1.8	209.9±2.0	NS	<0.0001	NS
Tibial Cancellous Microarchitecture									
BV/TV (%)	3.48±0.69	5.77±0.81	3.74±0.71	6.39±1.40	3.07±0.35	6.15±0.43	NS	0.0002	NS
Tb Th (□m)	42.98±1.01	47.48±1.72	40.44±1.05	48.10±1.52	41.60±1.58	50.61±1.37	NS	<0.0001	NS
Connectivity density	9.18±3.58	27.22±8.7	14.37±8.	33.55±13	6.28±1.7	26.25±3.	NS	0.0032	NS

	3	42	.21	5	54

UN=unstimulated, STI= stimulated